

Direct Lift Control: A review of its principles, merits, current and future implementations

Carmine Varriale ^a*,¹ Thomas Lombaerts ^b,² Gertjan Looye ^c

^a Delft University of Technology, Faculty of Aerospace Engineering, Delft, 2629 HS, The Netherlands

^b NASA Ames Research Center, Moffett Field, CA 94035, USA

^c German Aerospace Center (DLR), Institute of System Dynamics and Control, Weßling, 82234, Germany



ARTICLE INFO

Keywords:

Direct Lift Control
Pitch Attitude Control
Flight mechanics
Minimum phase system
Non-linear Dynamic Inversion
Control Allocation
Box-wing aircraft

ABSTRACT

Direct Lift Control (DLC) is the capability to directly and intentionally influence lift on a fixed-wing aircraft by means of aerodynamic control devices, with minimum change of its angle of attack. Although several definitions exist, with various degrees of ambiguity, the combination of DLC and pitch attitude control has unambiguously proven to reduce pilot workload and improve flying comfort considerably. DLC has historically seen several applications on so-called inflight simulators and, recently, this capability has been rolled out over several aircraft types of the US Navy fleet, massively reducing pilot workload during carrier landings. On the civil front, only one aircraft type has been equipped with this capability, despite its very positive reception by flight crews and passengers. The intention of this paper is to revive interest in civil DLC applications, by reviewing in-depth its basic principles, characteristic features, benefits, and implementations so far. Several modern aircraft and disruptive wing configurations appear to be inherently capable of accommodating DLC functionality from a flight physical, systems, and software point of view. The proven benefits of DLC are likely to well outweigh the cost of the added functionality.

Contents

1. Introduction	2
2. Basic principles of path and speed control	2
2.1. Attitude control vs. direct force control	3
3. Implementations	5
3.1. Transport aircraft	5
3.2. High-performance aircraft	6
3.3. Inflight simulators	7
4. Fundamental flight mechanics	8
4.1. Two conceptual examples	8
4.1.1. Pure heave evolution	9
4.1.2. Constant angle of attack evolution	10
4.2. General longitudinal response	11
4.2.1. Angle of attack dynamics	11
4.2.2. Numerical integration	11
4.2.3. Terminology	12
4.3. Properties of the Control Center of Pressure (CCoP)	12
4.3.1. Relation to the Overall Center of Pressure (OCoP)	12
4.3.2. Relation to the Instantaneous Center of Rotation (ICR)	13
4.3.3. Impact on trim angle of attack and speed stability	13

* Corresponding author.

E-mail address: C.Varriale@tudelft.nl (C. Varriale).

¹ Assistant Professor, Flight Performance and Propulsion Section.

² Aerospace Research Engineer, KBR Wyle Services, Intelligent Systems Division.

³ Head of Department, Department of Aircraft System Dynamics.

5. Control surface layouts	14
5.1. One control surface	15
5.1.1. Impact of spoilers location on dynamic response	16
5.2. Two control surfaces	16
5.2.1. Flying qualities and tracking precision	17
5.3. Multiple redundant control surfaces	17
5.3.1. Flight mechanics of staggered box-wing aircraft	18
6. Inflight demonstration	19
6.1. Flight control law architecture	19
6.2. Computer simulations	21
6.2.1. Tracking performance of DLC	21
6.2.2. Turbulence disturbance rejection of DLC	22
6.3. Flight tests	23
6.3.1. Experimental procedure	23
6.3.2. Experimental results	23
7. Conclusions	23
CRedit authorship contribution statement	24
Declaration of competing interest	24
Data availability	24
References	24

1. Introduction

DLC is the capability to directly and intentionally influence lift on a fixed-wing aircraft by means of aerodynamic control devices, with ideally no change in angle of attack and minimum change of moments about its body axes [1]. DLC has been a distinctive feature of the Lockheed-1011 Tristar, and made this aircraft stand out in (automatic) landing performance, handling qualities, and passenger comfort during the final approach phase [2]. Only more recently, DLC has proven to be a game-changer in improving landing performance and ease of piloting of high performance aircraft on carrier decks [3].

In light of the current interest in multi-functional wing trailing-edge devices [4] and disruptive configurations like box-wing aircraft [5], accommodating DLC on current and future aircraft may mainly necessitate adding software functionality. Such opportunity makes DLC possibly just too attractive to ignore, or even a necessity. Although the cost of adding functionality to certifiable control law software is very high, it may be more and more outweighed by the advantages of DLC that this paper intends to explore and review.

The objective of this paper is therefore to give an up-to-date overview of DLC, following up on [6] and addressing basic flight dynamics and control aspects, aerodynamics, control system architectures and implementations so far.⁴

The paper starts with the most high-level principles and motivation for using DLC in aircraft path and speed control. Then, a comprehensive overview of current and past applications in civil, military and experimental programs is given, followed by a more detailed discussion of the flight physical principles governing the operation of DLC.⁵ On those bases, control surface layouts and flight control law architectures with different ways of integrating Pitch Attitude Control (PAC) and DLC are discussed. These architectures are of generic nature and may therefore be applicable to future aircraft configurations.⁶ Finally, notable first-hand results from inflight tests are provided and discussed.⁷

⁴ The scope is limited to the use of aerodynamic control surfaces. Concepts like Powered Lift Control, Direct Thrust Control or applications achieving DLC through aerodynamic bleed [7] are not considered in this review.

⁵ The introduction to Section 4 and the content of Sections 4.1 to 4.2.2 are improvements on the authors' previous work.

⁶ Section 5.3 reviews the authors' previous work.

⁷ Section 6 reviews the authors' previous work.

2. Basic principles of path and speed control

Point-mass dynamics of fixed-wing aircraft velocity and flight path can be described using three equations [8]:

$$m\dot{V} = T - D - mg \sin \gamma \quad (1)$$

$$mV\dot{\gamma} = L - mg \cos \gamma \quad (2)$$

$$mV\dot{\chi} = L \sin \mu + Y \quad (3)$$

The variables are detailed in the list of symbols above, and may be referenced to an inertial frame or the air mass, assuming that wind velocity and direction is constant. On a fixed-wing aircraft, the control means to influence the main forces acting on the aircraft are:

- total engine thrust T , in Eq. (1);
- bank angle μ , in Eq. (3);
- angle of attack α , directly influencing the lift:

$$L \approx q_\infty S (C_{L_0} + C_{L_\alpha} \alpha) \quad (4)$$

- angle of sideslip β , directly influencing the side force:

$$Y \approx q_\infty S (C_{Y_0} + C_{Y_\beta} \beta) \quad (5)$$

The aerodynamic attitude angles α , β , and μ effectively serve as inputs to these equations, and they are realized and trimmed by means of moment-generating control surfaces. Most basically, neglecting dynamics and any cross couplings for lateral controls: a tail elevator is deflected to obtain a desired value of the trimmed angle of attack (and hence, of the trimmed airspeed) ($\alpha \sim \delta_{ele}$); a tail rudder is deflected to obtain a desired value (typically zero) of the trimmed sideslip angle ($\beta \sim \delta_{rue}$); ailerons are deflected to set the aircraft in a roll motion and retracted when a desired roll angle is obtained ($\mu \sim \delta_{ail}$).

The flight path and airspeed of fixed-wing aircraft is thus predominantly controlled by means of appropriate thrust setting and adjusting its attitude relative to the airflow. A number of observations can be made from the equations:

- Lateral flight path changes ($\dot{\chi} \neq 0$ in Eq. (3)) are achieved by directing the lift vector laterally by means of rolling the aircraft around its longitudinal body axis (actually: velocity vector), or by means of setting a sideslip angle. The latter is uncomfortable for passengers due to lateral acceleration, and tends to generate more drag. On transport aircraft it is therefore only used in case of engine failure or de-crab after a landing approach in cross winds.
- Speed changes ($\dot{V} \neq 0$ in Eq. (1)) are usually initiated by adjusting the thrust setting. Assuming a constant flight path angle ($\dot{\gamma} = 0$),

List of symbols		Subscripts and superscripts	
Roman letters			
<i>a</i>	Generic acceleration, m/s ²	ail	Aileron
<i>B</i>	Control effectiveness matrix, 1/rad	ele	Elevator
<i>C</i>	Dimensionless coefficient	ini	Initial condition
<i>c̄</i>	Aerodynamic mean chord, m	rud	Rudder
<i>D</i>	Drag force, N	spo	Steady state
<i>e</i>	Span efficiency factor	tr	Trim condition
<i>F</i>	Generic force, N	zl	Zero lift
<i>f</i>	Generic function		
<i>G</i>	Ganging matrix		
<i>g</i>	Gravitational acceleration, m/s ²		
<i>J</i>	Inertia tensor, kg m ²		
<i>L</i>	Lift force, N		
<i>L̄</i>	Roll moment, N m		
<i>M</i>	Mach number		
<i>m</i>	Mass, kg		
<i>M̄</i>	Pitch moment, N m		
<i>n</i>	Load factor		
<i>N̄</i>	Yaw moment, N m		
<i>p</i>	Roll rate, rad/s		
<i>q</i>	Pitch rate, rad/s		
<i>q̄</i>	Asymptotic dynamic pressure, Pa		
<i>r</i>	Yaw rate, rad/s		
<i>S</i>	Reference wing area, m ²		
<i>T</i>	Thrust force, N		
<i>t</i>	Time, s		
<i>u</i>	Longitudinal speed, m/s		
<i>ū</i>	Inputs		
<i>V</i>	Airspeed, m/s		
<i>w</i>	Vertical speed, m/s		
<i>X</i>	Longitudinal force, N		
<i>x_α</i>	Position of the neutral point, m		
<i>x</i>	States		
<i>x_δ</i>	Position of the Control Center of Pressure (CCoP), m		
<i>x_m</i>	Position of the maneuver point, m		
<i>Y</i>	Lateral force, N		
<i>Z</i>	Normal force, N		
Greek letters			
α	Angle of attack, rad		
β	Angle of sideslip, rad		
χ	Heading angle, rad		
δ	Control surface deflection, rad		
ϵ	Virtual control surface deflections, rad		
γ	Flight path angle, rad		
μ	Bank angle, deg		
ν	Control objective		
ω	Angular velocity, rad/s		
ρ	Radius of gyration, m		
τ	Time constant, s		
τ_{δ}	Control device efficiency		
δ	Pitch angle, rad		

in order to guarantee that lift remains approximately unchanged and keeps balancing the aircraft weight ($L = mg \cos \gamma \approx mg$), the angle of attack needs to be adjusted to compensate for changes in dynamic pressure (Eq. (4)). In the longer term, when a new steady-state airspeed is reached ($\dot{V} \rightarrow 0$), the final value of static thrust depends on the change in aerodynamic drag D , which is due to the desired change in airspeed and the necessary adjustment of the angle of attack.

- Vertical flight path changes ($\dot{\gamma} \neq 0$ in Eq. (2)) are usually initiated by changing the angle of attack, resulting in a change of lift and, consequently, acceleration normal to the trajectory. Assuming airspeed is held constant ($\dot{V} = 0$), when a new steady-state flight path angle γ is reached ($\dot{\gamma} \rightarrow 0$), the original angle of attack needs to be more or less restored since lift needs to balance the weight (see above). The thrust setting needs to be adjusted to compensate for the change in flight path angle ($\sin \gamma$ in Eq. (1)).

The initial and steady-state inputs on thrust setting and angle of attack to achieve desired changes of reference speed and flight path angle are thus largely opposite. For example, increasing airspeed while maintaining constant flight path angle requires increasing thrust and reducing angle of attack until a new steady-state. On the other hand, increasing the flight path angle at constant airspeed requires initially increasing the angle of attack, and later decreasing it to value lower than the initial one, while increasing steady-state thrust. This is due to the fact that the main forces acting on the aircraft are controlled by torque-generating devices, which couple the dynamics on different axes, and should be taken into consideration during the design of auto-flight functions [9].

2.1. Attitude control vs. direct force control

Flight path control of a fixed-wing aircraft via its attitude has proven to be highly effective, safe, and efficient. Control surfaces used to adjust

and hold attitude predominantly change moments around the aircraft body axes. They are positioned as far away from the Center of Gravity (CG) as practically possible, in order to keep the moment arms large and the control forces small. In this way, the use of the airframe attitude to take most of the responsibility of changing and maintaining its flight path and velocity can be achieved with relatively limited control power. Moreover, the control devices simultaneously maintain the attitude of the aircraft and, if necessary, stabilize it. The use of multiple devices (such as multiple elevators, rudders, ailerons) additionally allows for affordable redundancy and efficient trimming of the aircraft.

From a flight path tracking perspective, control via moment-generating devices has two disadvantages:

1. There is an inherent dynamic delay between the change of moments around the aircraft body axes and its effect on the flight path, since the resulting angular accelerations require — in mathematical terms — two integrations in time to result in the needed change of attitude.
2. This delay usually comes with non-minimum-phase behavior, since the control surfaces are located, on most aircraft, at the outer wings and at the tail empennage, the latter giving the aircraft natural static stability due to its aft position. When located behind the CG, the control forces needed to generate a required moment are always opposite to the intended direction of acceleration.

From a theoretical control point of view, this non-minimum-phase behavior puts an insurmountable limit on attitude control bandwidth and achievable tracking performance of vertical acceleration commands [10]. Such bandwidth limitation is a notorious issue in achieving accurate flight path tracking in severe turbulent conditions, such as during approach for landing. Increasing PAC bandwidth, if possible, directly goes at the cost of passenger and pilot comfort due to continuous change of attitude. On high performance aircraft, canards — all-moving surfaces positioned in front of the CG — are often used to avoid the non-minimum phase behavior, as the generated control forces always act in the same direction as the intended vertical acceleration. The destabilizing effect about the pitch axis increases the aircraft agility.

An alternative approach to improve flight path control capabilities consists in directly affecting the aircraft lift and drag via the deflection of over-the-wing spoilers:

$$L \approx q_{\infty} S \left(C_{L_0} + C_{L_a} \alpha + C_{L_{\delta_{spo}}} \delta_{spo} \right) \quad (6)$$

$$D \approx q_{\infty} S \left[C_{D_0} + k \left(C_L - C_{L_0} \right)^2 + \Delta C_D (\delta_{spo}) \right] \quad (7)$$

A steady spoiler deflection δ_{spo} is only capable of decreasing lift, and requires the angle of attack to be increased by $\Delta\alpha = - \left(C_{L_{\delta_{spo}}} / C_{L_a} \right) \delta_{spo}$ in order to maintain the lift required for vertical equilibrium (Eq. (6)). Such $\Delta\alpha$ is typically achieved by means of PAC with the tail elevator, and the maneuver results in an overall increase of induced drag, especially at higher angles of attack. The increase in drag due to spoiler deflection may be very significant for small airplanes (like gliders), while the lift contribution is usually more relevant for large airplanes, until the spoilers are completely raised and function as speed-brakes.

These principles are used on nearly all types of fixed-wing aircraft with the ultimate goal of increasing the steady-state angle of attack and/or thrust setting (Fig. 1). An example is provided by the Fly-By-Wire (FBW) spoiler system of the Boeing B737-MAX, which equips the aircraft with a “Landing Attitude Modifier” feature. The latter works as follows:

- for small flap deflections and low-thrust levels, spoilers are deflected to increase drag and enable above-idle thrust setting, which are instrumental to achieve steep descent at a relatively high airspeed;



(a) A glider using spoilers to directly manipulate drag and control the flight path angle during final approach.



(b) A Boeing B737-800 using spoilers to control the rate of descent.

Fig. 1. Aircraft configurations using over-the-wing spoilers during descent.
Source: Public domain and Wikimedia Commons, CC BY-SA 3.0 DEED

- for large flap deflections, spoilers are slightly deflected to reduce lift and drive the aircraft to a higher angle of attack, which is beneficial to ensure safe landing on the main landing gear [11].

Another example is provided by the high-lift system of the Airbus A350, which makes use of outboard flaps to optimize the wings lift distribution in cruise conditions [12]. This is achieved by coordinating the flap deflection with an over-the-wing spoiler droop deflection. The latter is enabled by a modification of the spoiler actuation system, which allows it to deploy downwards to follow the flap and increase the camber of the local airfoil. The flap is commanded independently by means of a dedicated Active Differential Gearbox (ADGB), and therefore acts as a primary control surface, although with reduced bandwidth [13].

The relevance of this approach can be grasped from Eqs. (1) and (2): in order to descend ($\gamma < 0$) and/or decelerate ($\dot{V} < 0$), the $T - D$ term must be made negative with the appropriate magnitude. When thrust is at idle (or fixed, or non-existent — as in the case of gliders), a direct alteration of drag is the only effective means remaining to achieve this condition. The coordinated use of spoilers and elevator allows direct manipulation of drag to achieve higher angles of attack and/or higher thrust setting (Eqs. (1)–(3) with subsequent discussion). By just employing PAC without spoilers, there would be no possibility to change drag without breaking vertical equilibrium.

A more versatile means of directly controlling lift is DLC. Borrowing from Pinsker [1], DLC can be defined as the capability to use “a control mechanism by which lift is generated [but more generally: “influenced”] without, or largely without, significant change in the aircraft incidence, and ideally is meant not to generate pitching moment”. Due to its inherent ability to adjust total lift in both directions (increasing



Fig. 2. Lockheed L-1011 Tristar during landing.
Source: Flickr, Aerolcarus, CC BY-SA 2.0 DEED.

and decreasing), DLC allows for direct vertical acceleration and flight path control on a short time scale.

As compared to the operation of spoilers discussed above, DLC is intended to be used dynamically rather than statically, as its purpose is to affect lift — and hence flight path — in the short-term transient response, instead of drag — and hence speed — in the longer term. This is usually achieved by washing out the DLC command δ_{DLC} with a time constant τ_{DLC} , so that

$$\Delta C_L \approx \begin{cases} C_{L_\alpha} \cdot 0 + C_{L_{\delta_{\text{DLC}}}} \delta_{\text{DLC}} + C_{L_{\delta_{\text{ele}}}} \Delta \delta_{\text{ele}}^{\text{ini}}, & t \ll \tau_{\text{DLC}} \\ C_{L_\alpha} \Delta \alpha + C_{L_{\delta_{\text{DLC}}}} \cdot 0 + C_{L_{\delta_{\text{ele}}}} \Delta \delta_{\text{ele}}^{\text{ss}}, & t \gg \tau_{\text{DLC}} \end{cases} \quad (8)$$

where $\Delta \delta_{\text{ele}}^{\text{ini}}$ is the elevator deflection used to initiate a change of angle of attack $\Delta \alpha$, and $\Delta \delta_{\text{ele}}^{\text{ss}}$ is the deflection needed to sustain $\Delta \alpha$ in the steady state. In the case speed was to be held constant, $\Delta \alpha$ would also have to be washed out via the elevator, in order to sustain the aircraft weight after returning to a steady vertical path (Eqs. (1)–(3) and subsequent discussion).

When $|C_{L_{\delta_{\text{ele}}}} \Delta \delta_{\text{ele}}^{\text{ini}}| < |C_{L_{\delta_{\text{DLC}}}} \Delta \delta_{\text{DLC}}|$, the aircraft response to changes in lift acquires minimum-phase behavior. The flight path bandwidth is then only limited by control surface actuation and structural aspects. Improving path tracking performance consequently improves — rather than compromises — passenger comfort, as this can be achieved without short-term attitude changes. Drag variations due to DLC deflections can be uncomfortable, though [14].

3. Implementations

Until recently, DLC has found very limited application, as added complexity, weight, and (maintenance) cost were considered not worth the benefits discussed above. Notable exceptions have historically been represented by the so-called inflight simulators.

For commercial aviation, DLC can be realized, to some extent, by means of conventional controls already available in most aircraft configurations, with over-the-wing spoilers and tail elevators being the best candidates to do so, by far. The best-known example to put this approach successfully in practice is the Lockheed 1011 Tristar, shown in Fig. 2. Other potential means of DLC are high-speed aileron or flaperon deflections, with some major caveats. Outboard ailerons are less suitable from a flight loads perspective, while in-board high-lift devices are not recommendable as their actuators tend to be incapable of following fast, dynamic commands [13].

For military aircraft, the situation has changed rapidly over the last few years. After initial applications on the F14 Tomcat, the US

Navy has re-introduced large-scale implementation of DLC as part of its Maritime Augmented Guidance with Integrated Controls for Carrier Approach and Recovery Precision Enabling Technologies (MAGIC CARPET) program. This consists in combining leading- and trailing-edge wing devices with elevator control surface deflections, hence achieving independent but coordinated pitch and vertical path control. This have proven to massively improve flight path tracking accuracy and dramatically reduce pilot workload during aircraft carrier landings [3].

Both on the Lockheed Tristar and the MAGIC CARPET system, PAC and DLC are applied in a complementary way. On a short time scale DLC is used to immediately respond to flight crew commands when tracking a reference path, or to compensate for turbulence. On a longer time scale, angle of attack is adjusted using classical controls, allowing DLC devices to return to their initial position. In this way, the aforementioned advantages of PAC and DLC augment each other very effectively.

When compared to the Lockheed Tristar, military and civil aircraft are nowadays controlled using Fly-By-Wire (FBW) and with the help of control augmentation algorithms. As demonstrated early on in [15] and proven now in practice by the MAGIC CARPET system, this makes optimal coordination of attitude and force control considerably easier.

A broad and detailed overview of DLC implementations is given in this section.

3.1. Transport aircraft

The best known aircraft to use DLC for commercial operations is with no doubt the Lockheed L-1011 TriStar [2,16]. This 200–230 ton, three-engine, wide-body airliner used its four inboard spoilers to employ DLC during final approach for landing. To this end, the spoilers were biased upwards in coordination with the full deployment of trailing-edge flaps, roughly canceling their respective effects on total lift but allowing fast maneuverability in the vertical axis. More specifically, the nominal set-point of the spoilers was raised to a ~10 deg deflection angle when flaps were extended to full position. From that condition, lift could be directly and quickly adjusted in both directions [2]. When mechanically coupled to the tail plane controls, this implementation made the longitudinal handling qualities, passenger comfort, and (automatic) landing performance of the aircraft in turbulence stand-out in comparison to other types of its time [2].

For the Lockheed TriStar, DLC was implemented to increase flight path control bandwidth, in order to improve the aircraft flight response to pilot commands, remove the non-minimum phase behavior, and reduce the aircraft sensitivity to external disturbances. It was integrated in the Flight Control System (FCS) through cross-feeds with the pitch control channel and the α -based auto-throttle, giving the L-1011 arguably the most advanced automatic landing system of its time. Results from simulated and piloted flights report a four-time reduction in the energy absorbed by gusts, significant reduction in touchdown dispersion, a two-fold reduction in touchdown vertical speed variance, increase in pilot acceptability, cost and weight savings due to a relief of the PAC system design requirements, “large improvements in terms of safety” and “vast improvement in ride comfort” [2].

Nelsen [17] integrated DLC into the experimental FBW of a B-52 long-range bomber to improve tracking during landing approach and inflight refueling. The system was successfully tested in a manned simulator [18]. Handling quality ratings were considerably higher compared with the original FCS, especially regarding effort, comfort, and precision in tracking speed.

Lorenzetti developed control laws using DLC with the help of optimization algorithms [19]. These were applied to models of the Boeing 27707 supersonic transport, a Lockheed C-5-like transport aircraft, as well as one representing a Boeing 747 aircraft.

Extensive studies on DLC were performed on the Boeing 367-80 (often referred to as the Boeing 707 prototype) [20–23]. A dedicated high-lift system based on spoilers and, in a next phase, adapted high-lift

flaps was designed and realized. Extensive simulation and flight tests were performed for modeling and validation purposes. Various studies were performed, using the DLC as part of the command augmentation system. The findings in [20] appear a bit less euphoric compared to all other applications.

Implementations to general aviation aircraft were studied by Kohlman in [6], also including flight test results on a Piper PA-24 aircraft using slot spoilers for lift adjustments. Interestingly, the paper also addresses direct side-force control.

König and Hahn developed a gust alleviation FCS for the Do-228 aircraft and DLR's VFW-Fokker 614-based inflight simulator AT-TAS (Advanced Technologies Testing Aircraft System) using symmetric aileron deflections, plus additional dedicated DLC surfaces in case of the latter [14]. The control laws used turbulence estimation at the aircraft nose, and computed open-loop compensatory control deflections. Very good improvements could be achieved, but a trade-off had to be made against drag variation caused by control deflection, resulting in annoying longitudinal accelerations and causing passenger discomfort.

Gerrits performed a study for a Cessna Citation-II aircraft, using fast actuators to move the flaps as lift control devices [24]. Classical control laws were developed to improve path tracking in turbulence. This work was in the frame of development of control technologies for a Dutch FBW test bed, and the actual aircraft is still in operation today, although without use of DLC [25].

Another study was performed by Merat, investigating the applicability of DLC to the Airbus A380, also inspired by the successful FCS of the Tristar. An authority of only 0.1 g was proven to render similar performance improvements in computer simulation studies [26].

Lombaerts and Looye developed and flight tested automatic flight control algorithms that exploit available DLC surfaces on DLR's AT-TAS [15]. The work contributed complementary integration of vertical acceleration control by means of PAC and DLC: acceleration commands were immediately tracked by commanding the latter and then washed out against appropriately adjusting the angle of attack.

Finally, Varriale made an in-depth review of the technology, and developed an alternative way of implementing DLC for an innovative box-wing aircraft [5].

3.2. High-performance aircraft

DLC has a long and rich history of various applications in high-performance aircraft, starting with some basic concepts in the 1960's which have evolved over the years into more advanced applications. Military applications of DLC are common in flight scenarios where maneuvering precision and response quickness are critical, like carrier-based landings or station-keeping for formation flight and inflight refueling.

The Vought F-8 Crusader carrier-based air-superiority supersonic jet aircraft, first flown in 1955, had a basic form of DLC. Flight path control at low approach speeds could not be accomplished with PAC alone and required use of the throttle as well, but engine response time was slow. DLC was flight tested on this configuration in the mid-1960's using ailerons as flaps. Drake presented an introduction to the Vought F8-C testbed with the cockpit architecture for DLC and how it impacted the stall margin [27]. Smith provided a review of the entire test program on that same testbed [28], and Stickle described the flight tests on an F8-C Crusader airplane which was modified to incorporate the aforementioned symmetrically variable ailerons as flaps [29].

The Grumman F-14 Tomcat carrier-capable variable-sweep wing supersonic fighter aircraft, first flown in 1970, employed a basic concept of DLC during carrier landings. DLC was used to control the vertical glide-slope angle without PAC inputs or engine throttle commands. DLC used the two inboard spoiler sections in conjunction with small corrections on the tail stabilizers, such that lift was controlled directly without rotations. DLC was engaged by depression of a dedicated switch on the control stick with flaps down and throttle less than

military power. This caused the inboard spoilers to extend to half, and enabled the DLC and maneuver flap command thumb-wheel on the control stick to control them. Such employment of DLC required the roll and pitch channels in the automatic FCS, the inboard spoilers and the hydraulic systems to be operative as well. Rotation of the thumb-wheel forwards extended the spoilers towards the max up position, decreasing lift and adjusting the glide-slope angle downward. Rotation of the thumb-wheel aft retracted the spoilers towards the flush position, increasing lift and adjusting the glide-slope angle upward. A further depression of the DLC switch disengages the system [30].

Fortenbaugh presented piloted simulations of 6-Degrees of Freedom (DoFs) carrier-based landings as part of a study on the augmentation of the Automatic Carrier Landing System (ACLS) of the F-14 A Tomcat with DLC capabilities [31]. DLC was achieved by the simultaneous use of trailing-edge flaps, in the last 10 s to 15 s of the landing maneuver. Two FCS architectures were compared, one with and one without DLC. A statistical comparison between landings was performed to evaluate flight control in the three main phases of the maneuver: approach, over-the-ramp, and touchdown. Results showed an astonishing 50% reduction in altitude and pitch attitude deviations, improved control of hook-to-ramp clearance and over-the-ramp pitch attitude, and improved control of touchdown attitude and touchdown point location, when using DLC. The use of DLC clearly yielded better and safer landings, and pilots ultimately recommended DLC for use in real ACLS operations. It was concluded that DLC "offers a state-of-the-art advance in performance with few additional expenditures of dollars and with insignificant aircraft weight and volume penalties" [31].

On the Lockheed S-3 Viking carrier-based anti-submarine warfare jet aircraft, first flown in 1972, DLC was implemented with the spoilers, which were biased up during landing to allow for subsequent direct changes in lift. The Viking possessed an unusual flight control system which combined six large spoilers with a set of small ailerons and a leading-edge flap. Lateral control was greatly aided by the inclusion of the spoilers in combination with the leading-edge flap, which permitted effective control at very low speeds with low engine power settings. All control surfaces on the aircraft were deflected using hydraulically-actuated servos, with an artificial feel system designed to give the pilot an idea of the extent of control surface deflection. These controls did however prove to be somewhat over-sensitive at high speed. Overall, the control surfaces were very effective on patrols at low speed, though they could prove rather clumsy in a carrier landing pattern. This was largely due to the over-powered engines, which gave the aircraft a somewhat unorthodox glide slope and its large wings increased its sensitivity to the "burble" air disruption behind the carrier. To compensate for this, the Viking was equipped with a dynamic DLC system which provided 12 deg of speed brake extension and retraction through the upper spoilers [32].

The 2015 landmark Maritime Augmented Guidance with Integrated Controls for Carrier Approach and Recovery Precision Enabling Technologies (MAGIC CARPET) project developed an enhanced set of flight control laws and Head-Up Display (HUD) symbology to drastically reduce pilot workload during carrier landings. It is nowadays referred to as Precision Landing Mode (PLM), and is described by Denham [3], while flight tests are elaborated upon by Shafer [33]. A key feature of the system is Integrated DLC, which significantly simplifies flying the typical carrier approach with the carrier's Optical Landing System (OLS) by allowing precise flight path changes via longitudinal stick inputs that directly command lift rather than pitching moment. Forward and aft stick commands modulate the ailerons and trailing-edge flaps in such a coordinated way to achieve DLC, while the pitching moment is canceled by the simultaneous horizontal tail commands. Additionally, a "Delta Path" control mode adds a feature that calculates a reference glide path at center stick deflection on the basis of glide-slope and ship speed. This allows the aircraft to capture, maintain, and return to the "ideal" 3.5 deg glide-slope, nearly hands-off. Only glide-slope deviations during approach are then corrected with longitudinal

stick inputs. As soon as the aircraft is back on profile, the stick is released, and the aircraft automatically maintains the reference glide path. This essentially decouples the glide-slope tracking task from the capture task. The enhanced HUD symbology provides much improved direct pilot feedback cues on the magnitude of glide-slope and lineup corrections. Shipboard flight tests in 2015 confirmed a 50% reduction in touchdown dispersion as well as greatly reducing overall carrier approach workload, as observed through real-time pilot feedback.

Similar performance demanded for carrier-based landings can also be expected for in-flight refueling operations. McNeill compares DLC to conventional pitch damping augmentation on a modified F-100C variable stability aircraft [34]. Flight tests were performed in 1973 with the objective to evaluate the handling qualities resulting from the two approaches for inflight refueling tasks. Three different aircraft system configurations were tested: the standard FBW control law, one with pitch damping augmentation, and one with DLC. DLC was achieved by symmetric actuation of the ailerons, which were additionally connected to the tail elevator. The gearing and ganging ratios were “optimized empirically for precision formation flying” [34]. Flight test results indicated a 19% decrease in vertical error and a 40% decrease in overall airplane motion for DLC, as compared to the base configuration. This improvement in performance resulted in a 1 to 2 rating point increase for handling qualities, turning the final evaluation from unsatisfactory to satisfactory. It was noted that DLC partially decoupled the vertical and pitch DoFs of the aircraft, thereby removing significant pitch oscillations while holding position and attitude. While the addition of DLC resulted in better station keeping during inflight refueling, the outcome was overall similar to installing classic pitch damping augmentation. Decisions on which method to adopt would have to rely on other considerations, such as ease of mechanization and/or feasibility due to the geometry of the aircraft.

More recent work on DLC for refueling and station-keeping was done with computer simulations only [35,36]. The former study focused on the development of a cooperative control system for a tanker and receiver aircraft, while the latter study developed an adaptive control system for a receiver aircraft. Both studies showed that DLC can be used to improve the performance of the receiver aircraft during refueling and station-keeping.

3.3. Inflight simulators

A special class of aircraft that uses both direct lift and direct side-force control is composed of the so-called inflight simulators. These aircraft are used to validate flight dynamic behavior and handling qualities of aircraft or concepts well before their first flight [37]. Inflight simulators typically require independent — instead of coordinated — control of vertical and attitude dynamics. This allows simulated state vector responses of virtual aircraft models to be mimicked by inflight simulators with relatively high accuracy.

An early example is the Lockheed L-1329 JetStar, operated by NASA during the 1970s [38]. Similarly, Princeton University operated their Princeton Variable-Response Research Aircraft, based on a modified North American Navion A [39,40]. Notable examples are the US company Calspan, which has a long history in operating inflight simulators, as well as the German Aerospace Center (DLR). A comprehensive overview of inflight simulators is given in [41].

DLR's flying test-bed ATTAS was operational from 1986 till 2011 and is based on a VFW 614, a 44-passenger civil transport aircraft (Fig. 3). The original conventional mechanical control system of the basic aircraft was supplemented with an electrical FBW FCS. Fig. 4 shows an overview of the aircraft and which control effectors can be steered through the FBW system. The evaluation pilot has a two-axes side-stick, shown in Fig. 5, FBW thrust levers, a landing flap lever, and programmable electronic primary and navigational displays available. The FBW systems architecture comprises full dual redundant control systems with four computers in each of both lanes. In addition to the standard control surfaces, ATTAS has six DLC flaps at the trailing edge of the landing flaps, as shown in Fig. 6. This aircraft has been the basis for the control system design and flight test described in Section 6.



Fig. 3. DLR's VFW-614 ATTAS in flight.
Source: DLR.

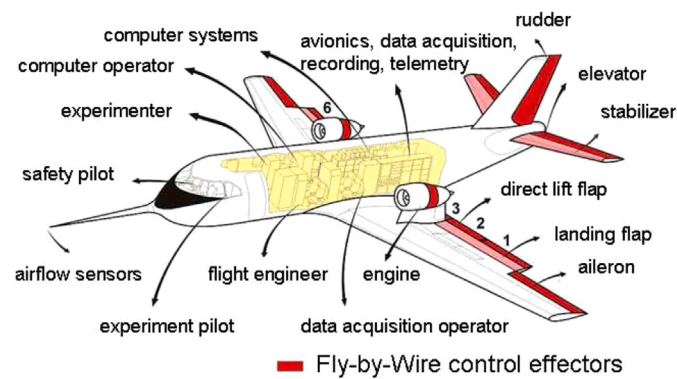


Fig. 4. An overview of the technical modifications incorporated in ATTAS. Besides the conventional elevator, rudder, and aileron control surfaces, the engines, six DLC flaps, landing flaps, and stabilizer are under fly-by-wire (FBW) control.
Source: DLR.



Fig. 5. ATTAS cockpit view, with experiment pilot seat on the left and safety pilot seat on the right.
Source: DLR.



Fig. 6. DLC flaps at the trailing edge of the wing on ATTAS.
Source: DLR.

4. Fundamental flight mechanics

DLC achieves the theoretically fastest control of the aircraft trajectory, for any aircraft that is capable to implement it. This is because the variation in lift is achieved by deflection of control surfaces, with little to no delay due to the alteration of the airframe incidence in the short term. As control surfaces can be actuated in a relatively short time frame, if the resultant control force caused by their deflection acts in proximity (ahead) of the aircraft CG, it instantly results in a translational acceleration which is only dependent on the aircraft mass. Such acceleration acts perpendicular to the airspeed vector — by definition of lift — and has the effect of curving the aircraft trajectory upwards or downwards. By neglecting unsteady aerodynamic effects and actuator dynamics, the dynamics of DLC can be expressed as in the following Eq. (9), where all the transformations occur at the same time-scale [15].

$$\delta_{\text{DLC}} \rightarrow \Delta L(\delta_{\text{DLC}}) \rightarrow \dot{\gamma} \propto 1/m \quad (9)$$

This is fundamentally opposed to PAC, which usually revolves around the use of a tail elevator to generate a small, dislocated control lift. In this case, such lift contribution is only relevant insofar it produces a significant pitch moment and gives raise to some angle of attack dynamics. In the case of PAC, the control lift generated by the elevator is used to alter the aircraft pitch moment, which in turn determines a change in attitude, angle of attack, and finally a variation of the lift generated by the airframe. This very indirect behavior ultimately results in some evolution of the aircraft trajectory, and it tends to become more sluggish with the increase of the aircraft moment of inertia about its lateral axis [1,2]. This is due to the fact that the magnitude of the delay between peak and steady-state response values to a PAC input is somewhat inversely proportional to the short-period time constant itself: the slower the short-period response, the more delay [42]. On larger aircraft, the FCS and control surfaces need to be dimensioned appropriately to compensate for this. The inherent lag of the trajectory response achieved with PAC should be evident from Eq. (10), where a change in flight path angle is achieved after two integrations in time.

$$\begin{aligned} \delta_{\text{ele}} &\rightarrow \Delta L(\delta_{\text{ele}}) \rightarrow \Delta M \rightarrow \\ &\rightarrow q \propto 1/J_y \xrightarrow{\int} \dot{\theta} \xrightarrow{\approx} \dot{\alpha} \xrightarrow{\int} \Delta \alpha \rightarrow \Delta L(\alpha) \rightarrow \dot{\gamma} \end{aligned} \quad (10)$$

The purpose of the upcoming discussion is twofold. Firstly, it intends to dissipate possible ambiguities stemming from different historical definitions of DLC, in order to clarify common misconceptions

around the unintuitive flight mechanics of its operation. This is done in Sections 4.1 and 4.2 by establishing that the most rigorous form of DLC must not be intended as resulting in pure heave motion (translation without rotation), because the latter implies that the angle of attack of the aircraft changes as a result of the translational motion imparted by the DLC input itself. Secondly, it provides a high-level theoretical framework to analyze the longitudinal response of an aircraft subject to a generic control input, independently from the FCS that is used to realize it in practice. This is done in Sections 4.3 and 4.3.3 by characterizing the properties of the Control Center of Pressure (CCoP) and relating them to other fundamental aerodynamic and dynamic loci. The CCoP is the application point of the lift due to control inputs only, and its non-dimensional position relative to the CG can be defined as in the exemplary Eq. (11), which is valid for a generic aerodynamic model which is linear in the controls.

$$\bar{x}_{\delta} = \frac{\sum_{i=1}^n C_{M_{\delta_i}} \delta_i}{\sum_{i=1}^n C_{L_{\delta_i}} \delta_i} \quad (11)$$

Although being quite impractical for closed-loop control, the concept of CCoP provides a fundamental ground to raise questions about where to position (redundant) control surfaces on the airframe, and how to coordinate their deflections in operation. This discussion is further expanded in Section 5.

4.1. Two conceptual examples

Consider a generic airframe, equipped with some sort of movable device which allows it to achieve different dynamic responses. Rather than focusing on the practical realization of such control device, the purpose of these examples is to show how different ways to generate control lift can impact the characteristics of the dynamic response.

The present analysis is only relevant for the transient response immediately after the control input, but some considerations are presented for the long term evolution for completeness. Some simplifying assumptions are adopted along the lines of classic derivations [1]. All angles are considered small, and a linear aerodynamic model with constant stability derivatives is adopted. The airspeed magnitude V_0 is assumed to stay constant during the maneuver. The effect of pitch rate q on the lift coefficient is neglected, as well as all higher order derivatives, unsteady effects due to $\dot{\alpha}$, and contributions that depend on the longitudinal development of the flow. The control input δ is assumed to happen instantaneously and, when positive, to result in an upward (or leftward, equivalently) shift of the lift curve of the airframe, which in turn results in an upward heave motion.

With these assumptions, the dynamics of the airframe in terms of variations from an initial equilibrium condition in straight and level flight — for example, $\alpha = \alpha(t) - \alpha^{\text{ini}}$ — are characterized by Eq. (12) when expressed with respect to the relative wind.

$$\left\{ \begin{array}{l} mV_0\dot{\gamma} = q_{\infty}S \left(C_{L_a}\alpha + C_{L_{\delta}}\delta \right) \\ J_y\dot{q} = q_{\infty}S\bar{c} \left(C_{L_a}\bar{x}_a\alpha + C_{L_{\delta}}\bar{x}_{\delta}\delta + C_{M_q}q \right) \\ \dot{\theta} = q \\ \alpha = \theta - \gamma \end{array} \right. \quad (12)$$

Lift due to the angle of attack of the airframe is applied at \bar{x}_a , which is the non-dimensional longitudinal position of the neutral point with respect to the position of the CG. The overbar notation signifies that such variable has been nondimensionalized with respect to the mean aerodynamic chord length \bar{c} . As already mentioned, \bar{x}_{δ} is the non-dimensional longitudinal position of the CCoP, which is the application point of lift generated directly by the control input. In general, it depends on the position of each available control surface, as well as on the combination of their deflections angles.

If quasi-steady equilibrium about the pitch axis is also assumed — $q \neq 0$ but $J_y\dot{q} \approx 0$ — the first two equations in Eq. (12) simplify to the

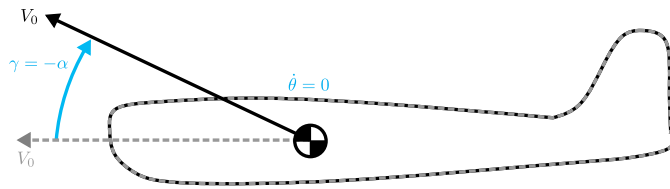


Fig. 7. Fundamental kinematics of simplified pure heave motion.

ones in Eq. (13), and it is possible to obtain closed-form solutions of the dynamic system analytically.

$$\begin{cases} mV_0\dot{\gamma} = q_\infty S \left(C_{L_a} \alpha + C_{L_\delta} \delta \right) \\ 0 = C_{L_a} \bar{x}_a \alpha + C_{L_\delta} \bar{x}_\delta \delta + C_{M_q} q \end{cases} \quad (13)$$

Throughout this entire section, it is going to be assumed that the deflection of any number of control surfaces can be coordinated by a suitable FCS, and that the resulting control forces and moments can be expressed as the result of one overall scalar input δ . An overview of methods that have been proposed in literature to actually perform this operation is presented in Section 5. In the two following examples, the dynamic evolution of the airframe starting out of a unit step on the input are assumed *a priori*. In this way, starting from the known vertical dynamics, it is then possible to determine the necessary position of the CCoP that achieves the desired motion of the airframe.

4.1.1. Pure heave evolution

For this example, it is assumed that a unit step on the input δ is able to impart pure heave motion to the airframe. The kinematics of an upward translation with no rotation are shown in Fig. 7. This motion type results in a decrease of the angle of attack which is due to the change in flight path angle. In particular, α is equal and opposite in sign to the variation of flight path angle γ , as summarized by Eq. (14).

$$q = \dot{\theta} = 0 \Rightarrow \dot{\alpha} + \dot{\gamma} = 0 \Rightarrow \alpha = -\gamma \quad (14)$$

During such maneuver, the lift coefficient increases because of the action of the control surfaces commanded by the input, but also decreases in light of the reduction of the angle of attack, as represented in Fig. 8(a). Because of this behavior, a pure heave maneuver should not be thought of as the ideal outcome of a DLC command, since part of the new lift generated by the control surfaces is lost by the reduction in angle of attack, which is a direct consequence of the necessity to maintain a constant pitch attitude.

By inserting Eq. (14) into Eq. (13), the system of equations of motion assumes the form reported in the following Eq. (15).

$$\begin{cases} mV_0\dot{\gamma} + q_\infty SC_{L_a} \gamma = q_\infty SC_{L_\delta} \delta \\ C_{L_a} \bar{x}_a \gamma = C_{L_\delta} \bar{x}_\delta \delta \end{cases} \quad (15)$$

The first equation shows that the dynamics of the flight path angle resulting from a control input δ have the characteristics of a linear first-order system with time constant t_a given by Eq. (16),

$$t_a = \frac{mV_0}{q_\infty SC_{L_a}} = \frac{mV_0}{L_a} \quad (16)$$

where mV_0 is the initial momentum of the aircraft and L_a is the lift slope of the airframe. The term proportional to the flight path angle γ indicates that the vertical dynamics is damped by aerodynamic forces due to the vertical motion of the airframe itself. The same equation allows to find the evolution of the flight path angle corresponding to the unit step input in an unequivocal manner. These are expressed in the following Eq. (17), and represented in Fig. 8(b).

$$\delta(t) = 1(t) \Rightarrow \begin{cases} \dot{\gamma}(t > 0) = \frac{C_{L_\delta}}{C_{L_a}} \frac{1}{t_a} e^{-t/t_a} \\ \gamma(t > 0) = \frac{C_{L_\delta}}{C_{L_a}} (1 - e^{-t/t_a}) \end{cases} \quad (17)$$

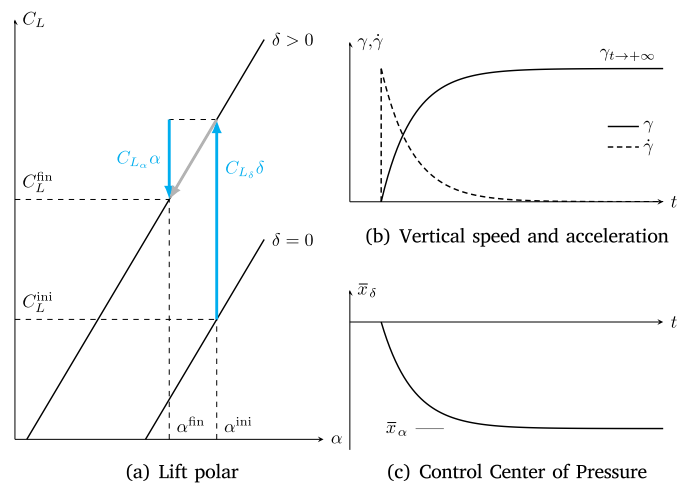


Fig. 8. Fundamental dynamics of simplified pure heave motion in response to a unit step input on the control device.

The dynamics of the flight path are sharp but damped, with exponential evolution, as expected. The initial rate response is given by the ratio of the lift effectiveness and the momentum of the airframe, as shown in Eq. (18).

$$\dot{\gamma}_{t \rightarrow 0^+} = \frac{L_\delta}{mV_0} \quad (18)$$

The trajectory bends upwards to the maximum achievable value of the steady-state, reported in Eq. (19), which depends on the efficiency of the control input $\tau_\delta = \partial \alpha_{zl} / \partial \delta < 0$.

$$\gamma_{t \rightarrow +\infty} = \frac{C_{L_\delta}}{C_{L_a}} = -\tau_\delta \quad (19)$$

The second line of Eq. (15) shows that also the position of the CCoP has to be, in general, a function of time in order to achieve the desired dynamics. It also shows that δ and \bar{x}_δ have the same dignity as input variables to control the vertical dynamics of the airframe. This is made evident by rewriting it in the form of Eq. (20), where both the control deflection and the position of the CCoP are in the same functional relation with respect to the flight path angle.

$$\bar{x}_\delta(t)\delta(t) = \frac{C_{L_a}\bar{x}_a}{C_{L_\delta}} \gamma(t) \quad (20)$$

This can be interesting for aircraft featuring redundant control surfaces, for which the instantaneous position of the CCoP depends both on the location of each movable surface and on the combination of their deflection angles. For these aircraft it could be possible, in principle, to achieve the same $\gamma(t)$ dynamics either by a time-varying input command $\delta(t)$ with a fixed CCoP position, or by a fixed input command which results in a time-varying position of the CCoP $\bar{x}_\delta(t)$.

By substituting the evolution of $\gamma(t)$ from Eq. (17) in Eq. (20), it is possible to formulate the condition required to obtain the pure heave type of dynamics. This is given by Eq. (21), which shows the position of the CCoP a function of time for a unit step input on $\delta(t)$. The time history of the CCoP position is shown in Fig. 8(c), assuming $\bar{x}_a < 0$ for a statically stable airframe.

$$\delta(t) = 1(t) \Rightarrow \bar{x}_\delta(t > 0) = \bar{x}_a (1 - e^{-t/t_a}) \quad (21)$$

For a unit step input, the CCoP has to move from its initial position at the CG ($t \rightarrow 0^+$) towards the neutral point of the airframe ($t \rightarrow +\infty$), behind the CG. The shift in position of the CCoP is necessary to counteract the decrease in pitching moment due to the decrease in angle of attack caused by the upward motion of the airframe. Before the control input is commanded ($t < 0$), the position of the CCoP is undefined because there are no control forces acting on the airframe.

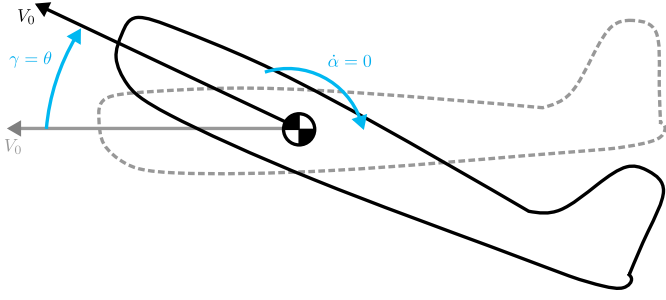


Fig. 9. Fundamental kinematics of simplified motion with constant angle of attack.

In summary, pure heave motion is characterized by a reduction of the angle of attack due to aerodynamic damping. It results in sharp but damped flight path angle response, for which the maximum value depends on the efficiency of the control input. If pure heave motion is desired, the center of pressure of the control lift has to timely move from the CG to the neutral point of the airframe. In free flight, this can be achieved — to some extent — by washing out an initial deflection of over-the-wing spoilers with a timely deflection of the tail elevator. The former would start the heave dynamics by generating a significant imbalance in lift force, but at the same time they would also create a (typically small) imbalance in the pitch moment with respect to the CG. The latter would then balance out the pitch moment, while generating only a small control lift that would not significantly affect the heave motion.

4.1.2. Constant angle of attack evolution

According to the definition reported at the beginning of this paper, a control input achieving DLC should result in no significant variation of the angle of attack. Assuming that the arising dynamics is characterized by no variation of α automatically implies that the airframe has to accompany the heave dynamics with some rotation about the pitch axis. In particular, the change in pitch attitude angle has to be equal in magnitude and sign to the change in flight path angle. This is shown in Fig. 9 and expressed by the following Eq. (22).

$$\dot{\alpha} = 0 \Rightarrow \dot{\theta} = q = \dot{\gamma} \quad (22)$$

With this control strategy, the airframe achieves no variation of lift due to variation in angle of attack, and the total lift and pitch coefficients are altered only by means of the control input. On the lift polar, it can be represented as in Fig. 10(a). By inserting Eq. (22) into Eq. (13), the original system of dynamic equations can be simplified to the one in Eq. (23).

$$\begin{cases} mV_0\dot{y} = q_\infty SC_{L_\delta}\delta \\ 0 = C_{L_\delta}\bar{x}_\delta\delta + C_{M_q}\dot{y} \end{cases} \quad (23)$$

As done in the previous example, solving the equation for vertical dynamics allows to obtain the response of flight path angle and rate to a unit step on the input. They are reported in Eq. (24), which shows that the angular rate is constant and equal to the ratio between the lift effectiveness of the control input and the airframe momentum.

$$\delta(t) = 1(t) \Rightarrow \begin{cases} \dot{y}(t > 0) = \frac{L_\delta}{mV_0} \\ \gamma(t > 0) = \frac{L_\delta}{mV_0}t \end{cases} \quad (24)$$

This is also the maximum rate obtainable in the case of pure heave motion. The trajectory bends upwards linearly with time. The lift slope of the airframe L_α has absolutely no role in this type of dynamics.

The characteristics of motion at constant angle of attack are graphically summarized in Fig. 10(b). From this figure, it should be clear that considerations related to long term dynamics are inconsistent with the assumptions of small angles made at the beginning of Section 4.1, and

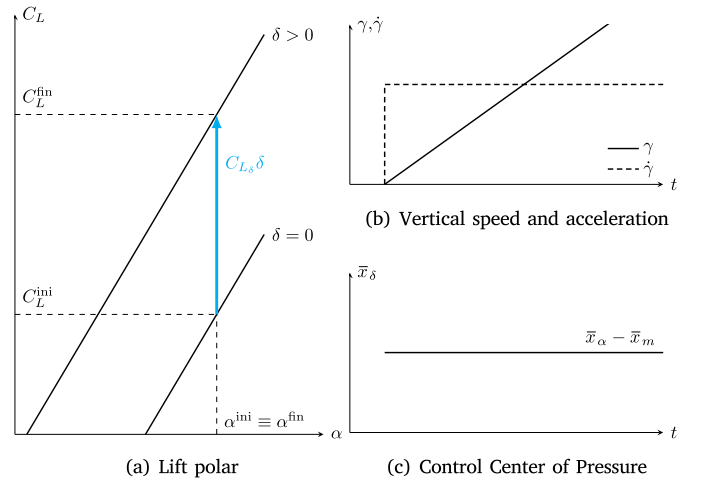


Fig. 10. Fundamental dynamics of simplified motion with constant angle of attack in response to a unit step input on the control device. This is the ideal outcome of Pure DLC.

in any case point to the fact that this type of motion is not suitable for long sustained maneuvers, as the rotation needed to neutralize the variation in angle of attack would be unbounded.

The condition required to achieve such type of dynamics is again obtained by substituting the newly found rate response into the second line of Eq. (23). Such condition is expressed by the following Eq. (25),

$$\delta(t) = 1(t) \Rightarrow \bar{x}_\delta(t > 0) = -\frac{q_\infty S}{mV_0} C_{M_q} \quad (25)$$

where the term on the right-hand side can be traced to a simplified expression of the maneuver margin \bar{x}_m [43]. This is the distance between the maneuver point and the CG of the airframe, and can be expressed as in the following Eq. (26).

$$\bar{x}_m = \bar{x}_\alpha + \frac{q_\infty S}{mV_0} C_{M_q} \quad (26)$$

Combining the previous two equations shows that, in order to achieve longitudinal dynamics at constant angle of attack, the control input must be able to drive the CCoP to a position which falls fore of the neutral point by a distance equal to the maneuver margin. This is expressed in the following Eq. (27), and the simple time history of the position of the CCoP is shown in Fig. 10(c).

$$\delta(t) = 1(t) \Rightarrow \bar{x}_\delta(t > 0) = \bar{x}_\alpha - \bar{x}_m \quad (27)$$

For a unit step input, the CCoP has to lie at this critical position from the instant in which the control is active ($t \rightarrow 0^+$) throughout the entire maneuver ($t \rightarrow +\infty$). As in the previous example, the position of the CCoP is undefined before the control input is commanded ($t < 0$).

In summary, motion at constant angle of attack is characterized by a pitch rotation that accompanies the vertical dynamics of the airframe. It results in a sharp, constant rate of change of the flight path angle, which makes the airframe very agile throughout the entirety of a short term transient response. If motion at constant angle of attack is desired, the center of pressure of the control lift has to act a maneuver margin fore of the neutral point of the airframe. In free flight, this can be achieved — to some extent — with the use of canard wings or leading-edge devices on the main wing, possibly in combination with over-the-wing spoilers. An increase in control lift due to a canard wing deflection, for example, would be accompanied by a positive pitch rotation which would counteract the decrease in angle of attack due to the upward motion of the airframe triggered by the lift imbalance due to the canard deflection itself. The deflection of over-the-wing spoilers would reduce or neutralize such lift imbalance in magnitude, while generating a small control moment that would not significantly affect the rotation imparted by the canard.

4.2. General longitudinal response

Moving on the path traced by the latter two examples, it should feel intuitive to envision a type of longitudinal response for which the rotation of the airframe contributes positively to the lift generated by the control input. In such a case, the flight path rate response would benefit from an initial contribution due to control-dependent lift, and then from an additional boost due to angle of attack.

In this section, the general vertical response to a control input is discussed in simplified hypotheses. First, the equation for angle of attack dynamics is derived and discussed. Then, a more general set of longitudinal equations of motion, coupled with a linear aerodynamic model, are numerically integrated to obtain graphical results.

4.2.1. Angle of attack dynamics

A more general equation for the longitudinal dynamics can be obtained from Eq. (13) by imposing the following kinematic relation, valid for any evolution in a vertical plane.

$$q = \dot{\theta} = \dot{\gamma} + \alpha \quad (28)$$

The resulting dynamics of the angle of attack, which couples vertical and rotational evolutions, is expressed in Eq. (29).

$$\left(\frac{C_{M_q}}{\bar{x}_m} \right) \dot{\alpha} + C_{L_\alpha} \alpha = \left(\frac{\bar{x}_\alpha - \bar{x}_\delta}{\bar{x}_m} - 1 \right) C_{L_\delta} \delta \quad (29)$$

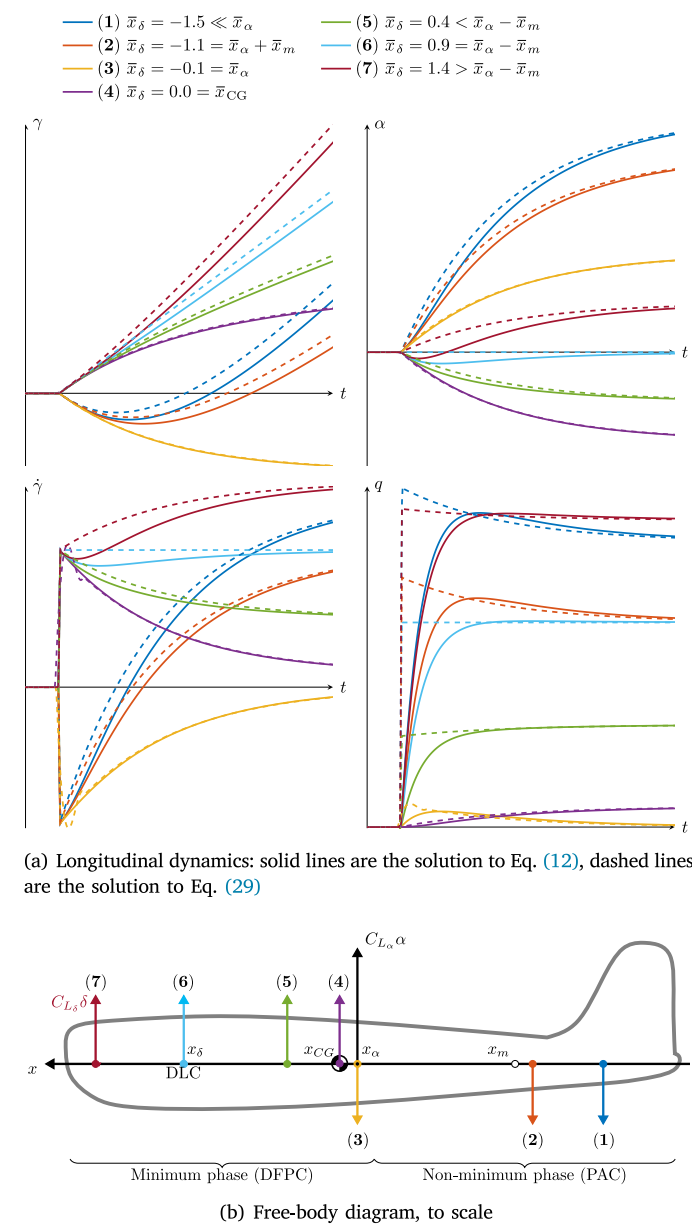
Even without solving it numerically, a few things can be noticed from this expression. First, the numerator of the gain of the input term is the relative position of the CCoP with respect to the neutral point of the airframe. It does not depend on the position of the CG, and it majorly influences the vertical response in both sign and magnitude [1]. Secondly, the maneuver margin at the denominator plays the role of a scale factor, both for the distance between the CCoP and the neutral point, and for the rate of change of the angle of attack. The higher the maneuver margin, with everything else being constant, the lower the gain of the input term, and the slower the angle of attack response. The absolute position of the CG impacts the static and maneuver margins of the aircraft, \bar{x}_α and \bar{x}_m , but not necessarily the position of CCoP, as the latter depends on the location and deflection of all control surfaces involved in the maneuver.

4.2.2. Numerical integration

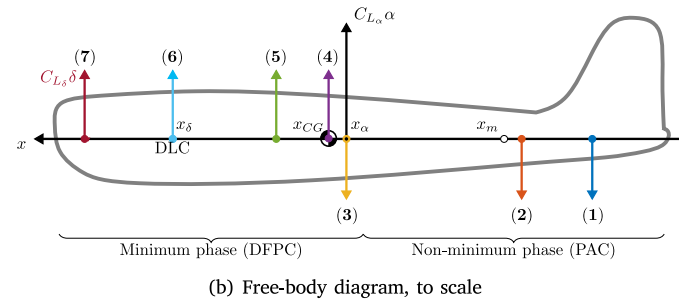
The dynamic response of the airframe is now obtained explicitly for various positions of the CCoP. Similarly to the derivation provided in [1], it is supposed that an abstract control device is able to achieve any desired position of the CCoP, but in this case all of the airframe parameters are retained fixed. Both the general equations of motion reported in Eq. (12) and the simplified ones of Eq. (29) are solved numerically for an abstract airframe with $\bar{x}_\alpha = -0.1$ and $\bar{x}_m = -1$, and for assigned notable positions of the CCoP. The lift contribution due to pitch rotation C_{L_q} is still neglected, as it does not alter the results or any conclusion.

The dynamic responses to the step input highlight significantly different behaviors as the assigned position of the CCoP moves from the tail to the nose of the airframe. They are shown in Fig. 11 in the case of a pull-up maneuver, with reference to the following discussion:

- (1-2) When the CCoP is located aft of the neutral point the initial and final flight path rate responses are discordant in sign. A pull-up maneuver results in the airframe initially plunging downwards and pitching up. This corresponds to the undesired non-minimum phase typical of PAC.
- (3) As the CCoP moves from the tail towards the neutral point, the magnitude of the steady-state flight path rate decreases, until reaching a minimum value of zero when the CCoP coincides with the neutral point. The time to achieve a certain angle of



(a) Longitudinal dynamics: solid lines are the solution to Eq. (12), dashed lines are the solution to Eq. (29)



(b) Free-body diagram, to scale

Fig. 11. Dynamic response of a generic airframe to a unit step input for different imposed positions of the CCoP. Static margin $\bar{x}_\alpha = -0.1$, maneuver margin $\bar{x}_m = -1$.

attack increases, the maximum angle of attack achievable decreases, and flight path tracking performance overall degrades. A proper pull-up maneuver with the CCoP coinciding with the neutral point would require an input on the control device in the opposite direction of the previous cases.

- (4) If the CCoP is located slightly fore of the neutral point, the initial and steady-state flight path responses are concordant in sign. A pull-up maneuver results in an initial upward acceleration, accompanied by a gentle pitch rotation up to a small constant angular speed. A longitudinally stable aircraft can achieve this behavior if the CCoP coincides with the CG.
- (5) As the CCoP moves forward of the neutral point up to a distance equal to the maneuver margin, the magnitude of the angle of attack response is reduced over time, as the pitch-up rotation is more effective at overcoming the aerodynamic damping due to the heave motion.

- (6) If the CCoP lies fore of the neutral point by a distance exactly equivalent to the maneuver margin, the steady-state flight path rate and angle of attack are equal to the initial ones. The control force acts in the same direction of the desired motion, and its moment arm is sufficiently large to trigger a pitch rotation that is able to neutralize the aerodynamic damping due to the heave motion. The airframe moves up and pitches up in a way to experience virtually no variation in the angle of attack. Such behavior coincides with the one that has been presented in Section 4.1.2.
- (7) By further advancing the CCoP, the dynamics of the angle of attack tend to further feed the initial response to the control input. The control lift lies sufficiently fore of the CG to trigger a significant pitch up rotation, which increases the angle of attack in a similar way as PAC would do, but with minimum phase response of the flight angle.

4.2.3. Terminology

The evolutions corresponding to cases (4)–(7) could be regarded as the most effective ways to employ the lift-generating capabilities of both the airframe and the control input for flight path control purposes. For this reason, “DLC” was originally used as an umbrella term to generically refer to these types of evolutions. In particular, the evolution of case (6) was indicated as “Pure DLC”, since the capability to generate airframe lift with changes in the angle of attack is completely unexploited. These definitions have been historically accompanied with the expectation that DLC “ideally is meant not to generate pitching moment” [1].

In light of the results shown in the previous sections, it is clear that the combination of the two classic definitions is impossible, and, together with the adopted terminology, leads to ambiguity and confusion in the interpretation of the phenomenon that the terminology tries to capture. Fig. 11(a) shows that it is impossible to achieve both no variation in angle of attack and no alteration of pitch moment ($C_M \propto \dot{q}$). The so-called “Pure DLC” achieves (almost) no variation in α with control lift acting a maneuver margin fore of the neutral point, but results in a sharp initial pitch-up rotation of the airframe. On the other hand, in order to achieve (almost) no variation in pitch moment with respect to the CG, the control force has to act at the CG itself, and the angle of attack reduces over time.

In light of this, we believe it is more appropriate to indicate the evolutions corresponding to cases (3)–(7) with the term Direct Flight Path Control (DFPC), since all of them result in a minimum-phase response of the flight path angle. Among them, case (6) is the only one which achieves DFPC with no variation in angle of attack, and hence should be referred to as DLC. These definitions are also indicated in Fig. 11(b). The adjective “pure” is therefore redundant and should be discarded for DLC, in the same way as there is no such thing as “pure” PAC.

4.3. Properties of the Control Center of Pressure (CCoP)

In the previous sections, it has been assumed that the position of the CCoP can be assigned arbitrarily and can be held constant throughout the dynamic evolution of the airframe, while in fact it is a function of many flight and control parameters. In this section, the theoretical properties of the CCoP are characterized in a general and fundamental way, and expressions are derived to relate it to other fundamental loci on a moving airframe.

To enable a mathematical definition of the CCoP, the model used to represent the aerodynamic actions due control surfaces has to be separable from the one used to describe the actions due to the clean aerodynamics of the airframe. A generic model which complies with this requirement is shown in Eq. (30), where the \mathcal{A} superscript indicates the aerodynamics of the airframe, and the \mathcal{C} superscript indicates

control actions.

$$\begin{cases} C_M = C_M^{\mathcal{A}}(\alpha) + C_M^{\mathcal{C}}(\alpha, \delta) \\ C_L = C_L^{\mathcal{A}}(\alpha) + C_L^{\mathcal{C}}(\alpha, \delta) \end{cases} \quad (30)$$

If the two sets of actions, and the underlying pressure fields, can be imagined as completely separable, they can be reduced to two independent centers of pressure. The dimensionless position of the Aerodynamic Center of Pressure (ACoP) — the application point of all actions due to the clean aerodynamics only — with respect to the CG is shown in Eq. (31), and is a function of the angle of attack only. More in general, it is a function of all flight parameters related exclusively to the airframe.

$$\bar{x}_p^{\mathcal{A}} = \frac{C_M^{\mathcal{A}}(\alpha)}{C_L^{\mathcal{A}}(\alpha)} = \bar{x}_p^{\mathcal{A}}(\alpha) \quad (31)$$

The dimensionless position of the CCoP with respect to the CG is calculated as in Eq. (32), and is a function of both α and δ . More generally, it is a function of all flight and control parameters. It has already been introduced with the symbol \bar{x}_δ .

$$\bar{x}_\delta = \bar{x}_p^{\mathcal{C}} = \frac{C_M^{\mathcal{C}}(\alpha, \delta)}{C_L^{\mathcal{C}}(\alpha, \delta)} = \bar{x}_\delta(\alpha, \delta) \quad (32)$$

The position of the Overall Center of Pressure (OCoP) — the application point of the total aerodynamic action on the airframe — can then be expressed as in Eq. (33).

$$\bar{x}_p = \frac{C_M}{C_L} = \bar{x}_p^{\mathcal{A}} + \frac{C_L^{\mathcal{C}}}{C_L} (\bar{x}_\delta - \bar{x}_p^{\mathcal{A}}) = \bar{x}_p(\alpha, \delta) \quad (33)$$

4.3.1. Relation to the Overall Center of Pressure (OCoP)

If there exists one combination of control surface deflections δ^* that is able to drive the CCoP to coincide with the ACoP at a given angle of attack, then the position of the CCoP — as well as the one of the OCoP — does not depend on control parameters at that angle of attack. This is shown in Eq. (34).

$$\bar{x}_\delta(\alpha, \delta^*) = \bar{x}_p^{\mathcal{A}}(\alpha) \Rightarrow \begin{cases} \bar{x}_p(\alpha, \delta^*) = \bar{x}_p^{\mathcal{A}}(\alpha) \\ \left. \frac{\partial \bar{x}_\delta}{\partial \delta} \right|_\alpha = \left. \frac{\partial \bar{x}_p^{\mathcal{A}}}{\partial \delta} \right|_\alpha = \left. \frac{\partial \bar{x}_p}{\partial \delta} \right|_\alpha = 0 \end{cases} \quad (34)$$

Such flight condition provides an opportunity to coordinate the deflection of different control surfaces while leaving the position of the center of pressure unaltered. Such operation should be carried out at the constant angle of attack α , in order not to affect the position of the ACoP.

The opposite statement is in general not true: if the CCoP is independent of the control surface deflections, it does not necessarily coincide with the ACoP. Moreover, the fact that it does not depend on control parameters is not sufficient to make the OCoP independent of control parameters as well. The variation of the OCoP with control surface deflections is shown in Eq. (35), where its relation to the CCoP can also be appreciated.

$$\frac{\partial \bar{x}_p}{\partial \delta} = \frac{C_L^{\mathcal{A}}}{C_L^2} \frac{\partial C_L^{\mathcal{C}}}{\partial \delta} (\bar{x}_\delta - \bar{x}_p^{\mathcal{A}}) + \frac{C_L^{\mathcal{C}}}{C_L} \frac{\partial \bar{x}_p}{\partial \delta} \quad (35)$$

It can be observed that \bar{x}_p is independent of control inputs either if $\bar{x}_\delta = \bar{x}_p^{\mathcal{A}}$ (as in Eq. (34)), or if both the CCoP and the lift coefficient are independent of control inputs themselves. The latter condition, expressed in Eq. (36), represents a criterion to guide the coordination of multiple control surface deflections without altering the position of the OCoP of a given airframe.

$$\left. \begin{array}{l} \bar{x}_\delta \neq \bar{x}_p^{\mathcal{A}} \\ \frac{\partial \bar{x}_\delta}{\partial \delta} = 0 \\ \frac{\partial C_L^{\mathcal{C}}}{\partial \delta} = 0 \end{array} \right\} \Rightarrow \frac{\partial \bar{x}_p}{\partial \delta} = 0 \quad (36)$$

Note that it is impossible to fulfill this condition with only one control surface, unless it is completely ineffective.

4.3.2. Relation to the Instantaneous Center of Rotation (ICR)

By definition, the Instantaneous Center of Rotation (ICR) of a rigid body is the only point in the field of motion of the body which instantaneously has zero velocity. Thus, at any given instant, the rigid body appears to be rotating about the ICR. The ICR can or cannot belong to the rigid body itself and, in general, its position changes in time [44,45].

The instantaneous velocity of every point rigidly connected to the aircraft is expressed as in the following Eq. (37),

$$\mathbf{V} = \mathbf{V}_{\text{CG}} + \boldsymbol{\omega} \times \mathbf{x} \quad (37)$$

where \mathbf{x} is the position of the given point with respect to the CG. The instantaneous position of the ICR can then be obtained by imposing $\mathbf{V} = \mathbf{0}$. For a rigid aircraft moving with wings leveled in a vertical plane, with linear velocity $\mathbf{V}_{\text{CG}} = [u, 0, w]$ and angular velocity $\boldsymbol{\omega} = [0, q, 0]$ in body axes, this results in the coordinates of the ICR reported in Eq. (38), which depend on the combination of the translational and rotational motion of the aircraft.

$$x_{\text{ICR}} = \frac{w}{q} \quad z_{\text{ICR}} = -\frac{u}{q} \quad (38)$$

If the aircraft is not rotating, as it happens in trimmed flight or pure heave motion, the ICR is not defined, and it is conventionally said to lie infinitely far away from the body. If the aircraft is purely rotating, with no forward or vertical speed, the ICR coincides with the CG. It is obviously impossible to obtain the latter condition in any realistic flight scenario.

The instantaneous variation in the position of the ICR is expressed in (39).

$$\dot{x}_{\text{ICR}} = \frac{\dot{w} - \dot{q}x_{\text{ICR}}}{q} = u + \frac{1}{q} \left(\frac{Z}{m} - \frac{\mathcal{M}}{J_y} x_{\text{ICR}} \right) \quad (39a)$$

$$\dot{z}_{\text{ICR}} = -\frac{\dot{u} + \dot{q}z_{\text{ICR}}}{q} = w - \frac{1}{q} \left(\frac{X}{m} + \frac{\mathcal{M}}{J_y} z_{\text{ICR}} \right) \quad (39b)$$

The term in parentheses on the right-hand side of Eq. (39a) is the vertical acceleration perceived in body axes at a point horizontally aligned with the aircraft CG ($z = 0$) and vertically aligned with the ICR ($x = x_{\text{ICR}}$). In case of a linear aerodynamic model with only one control effector — similar to the one previously shown in Eq. (13) — such acceleration can be expressed as in Eq. (40) for any point lying on the aircraft longitudinal body axis.

$$a_z(x, z=0) = \frac{Z}{m} - \frac{\mathcal{M}}{J_y} x = \\ = Z_a \left(\frac{1}{m} - \frac{x_a x}{J_y} \right) \alpha + Z_\delta \left(\frac{1}{m} - \frac{x_\delta x}{J_y} \right) \delta - \frac{\mathcal{M}_q q}{J_y} x \quad (40)$$

In these hypotheses, such acceleration is independent of the control input only if it is measured at the position x^* indicated in Eq. (41), where ρ_y is the radius of gyration about the lateral body axis.

$$x^* = \frac{J_y}{m x_\delta} = \frac{\rho_y^2}{x_\delta} \quad (41)$$

In this case, x^* is a fixed position with respect to the airframe, and it belongs within the airframe only if \bar{x}_δ is large enough. Measuring the normal acceleration in this position can be relevant for applications that rely on the normal load factor as a feedback control signal [46].

4.3.3. Impact on trim angle of attack and speed stability

For a given aircraft weight, the lift coefficient required to guarantee vertical equilibrium in trimmed flight C_L^{tr} is inversely proportional to the square of the airspeed V . This means that C_L^{tr} has to decrease if it is desired to fly in equilibrium at higher speeds, and it has to increase if it is desired to fly in equilibrium at lower speeds, as shown in the following Eq. (42).

$$C_L^{\text{tr}} = \frac{2mg}{\rho V^2 S} \Rightarrow \frac{dC_L^{\text{tr}}}{dV} = -\frac{4mg}{\rho V^3 S} = -\frac{2C_L^{\text{tr}}}{V} < 0 \quad (42)$$

In order to understand how such change in lift coefficient should be realized in practice, it is necessary to also examine the pitch equilibrium

equation. This is shown in the following Eq. (43) for a generic linear aircraft model for which the control actions can be reduced to a single force acting at \bar{x}_δ [1,43].

$$\begin{cases} C_L(\alpha, \delta) = C_{L_0} + C_{L_\alpha} \alpha + C_{L_\delta} \delta = C_L^{\text{tr}} = 2mg/\rho V^2 S \\ C_M(\alpha, \delta) = C_{M_0} + C_{L_\alpha} \bar{x}_\alpha \alpha + C_{L_\delta} \bar{x}_\delta \delta = C_M^{\text{tr}} = 0 \end{cases} \quad (43)$$

By solving the pitch trim equation for δ and substituting the latter expression in the first equation, it is possible to obtain the expression of the lift coefficient required to trim the aircraft for both vertical and rotational equilibrium in symmetric flight (Eq. (44)).

$$C_L^{\text{tr}} = \underbrace{\left(C_{L_0} - \frac{C_{M_0}}{\bar{x}_\delta} \right)}_{C_{L_0}^{\text{tr}}} + \underbrace{C_{L_\alpha} \left(1 - \frac{\bar{x}_\alpha}{\bar{x}_\delta} \right) \alpha^{\text{tr}}}_{C_{L_\alpha}^{\text{tr}}} = \frac{2mg}{\rho V^2 S} \quad (44)$$

The latter equation is an “operational” or “trimmed” lift curve, which represents the aerodynamics of the aircraft in its actual operating conditions in equilibrium flight. In the $C_L(\alpha, \delta)$ carpet plot, it identifies the locus of angles of attack and lift coefficients that are actually achievable in equilibrium flight, given that a control input δ is deployed at the location \bar{x}_δ to trim the aircraft about its pitch axis. Eq. (44) clearly shows that both the lift coefficient at zero angle of attack and the lift slope necessary to trim the aircraft ($C_{L_0}^{\text{tr}}$ and $C_{L_\alpha}^{\text{tr}}$) depend on the application point of the control input \bar{x}_δ .

The trimmed lift slope $\frac{dC_L^{\text{tr}}}{d\alpha^{\text{tr}}} = dC_L^{\text{tr}}/d\alpha^{\text{tr}} dV$ can be used to obtain a relation between the required change in trim angle of attack and flight airspeed. This is shown in the following Eq. (45), making use of Eq. (42).

$$\frac{dC_L^{\text{tr}}}{dV} = \frac{dC_L^{\text{tr}}}{d\alpha^{\text{tr}}} \frac{d\alpha^{\text{tr}}}{dV} \Rightarrow \frac{d\alpha^{\text{tr}}}{dV} = -\frac{2C_L^{\text{tr}}}{VC_{L_\alpha}^{\text{tr}}} = \frac{2\bar{x}_\delta C_L^{\text{tr}}}{VC_{L_\alpha}(\bar{x}_\alpha - \bar{x}_\delta)} \quad (45)$$

The latter shows that the angle of attack of the aircraft exhibits different behaviors with respect to airspeed, depending on the positions of the CCoP relative to the CG and/or to the neutral point [1].

The relations derived in the previous paragraphs are summarized in Fig. 12, assuming a statically stable aircraft with a fixed static margin $\bar{x}_\alpha = -0.1$. With reference to the following discussion, Fig. 12(a) shows the ratio between the trimmed lift slope and clean lift slope as a function of \bar{x}_δ , Fig. 12(b) shows the trim lift coefficient curves for different values of \bar{x}_δ as compared to the untrimmed ones, and Fig. 12(c) shows the variation of trim angle of attack with respect to airspeed as a function of \bar{x}_δ . The following theoretical cases can be identified:

- (1) $\bar{x}_\delta < \bar{x}_\alpha \Rightarrow 0 < C_{L_\alpha}^{\text{tr}}/C_{L_\alpha} < 1$ — If the CCoP falls aft of the neutral point, using the control input to trim the aircraft reduces the usable lift slope of the airframe. To maintain a given lift coefficient, the aircraft requires a larger angle of attack than if it was in clean configuration. For this reason, the lift coefficient actually achievable in equilibrium flight is bounded by the maximum (stall) angle of attack, and is lower than the clean $C_{L_{\max}}$. In other words, the aircraft is not able to exploit the entire C_L range — from 0 to $C_{L_{\max}}$ — using the control authority which is in principle made available by the control input excursion $[\delta_{\min}, \delta_{\max}]$. At the same time, because $d\alpha^{\text{tr}}/dV < 0$, an increase in airspeed requires a decrease in trim angle of attack, which is the most classic and intuitive piloting strategy. PAC and tailless aircraft configurations equipped only with trailing-edge control devices fall in this range of operations. The further aft the CCoP falls, the lower this effect is, as the increased moment arm enables a decrease in control lift to achieve trim. The closer \bar{x}_δ is to the neutral point, the more significant such reduction is.
- (2) $\bar{x}_\delta = \bar{x}_\alpha \Rightarrow C_{L_\alpha}^{\text{tr}} = 0$ — In the limit case of the CCoP coinciding with the neutral point, the usable lift slope in equilibrium conditions is null. The aircraft is not able to achieve any trim lift coefficient different from the one of the bare airframe $C_L^{\text{tr}} = C_{L_0} - C_{M_0}/\bar{x}_\alpha$, which could only be realized at one

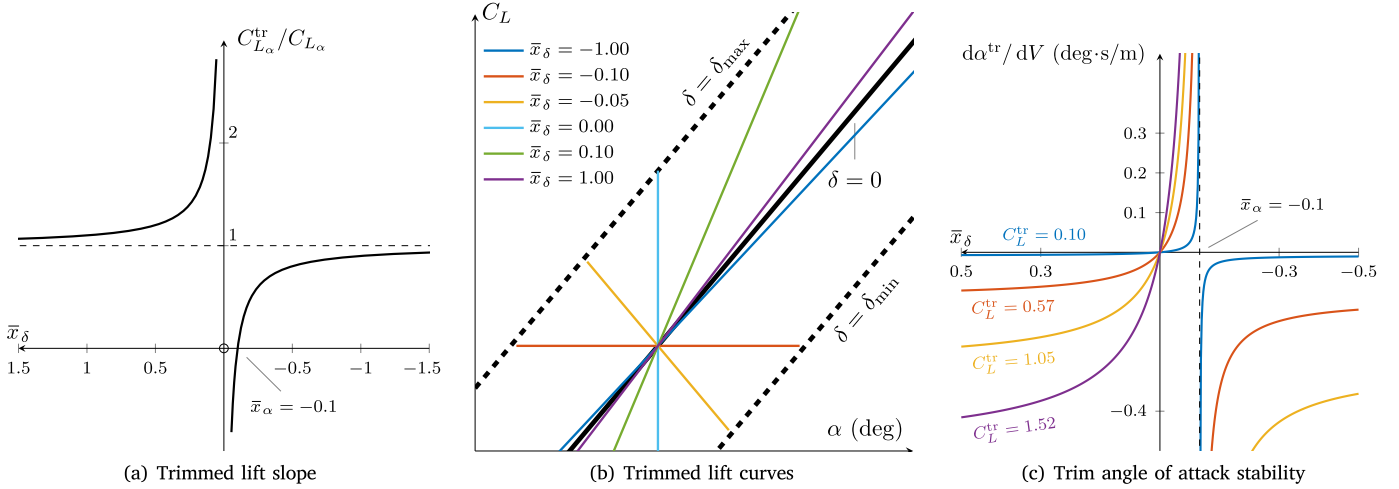


Fig. 12. Variation of trim parameters for different positions of the CCoP, for a generic statically stable aircraft with a fixed stable static margin $\bar{x}_\alpha = -0.1$.

value of the airspeed. Any variation in airspeed would require an infinite change in angle of attack to maintain equilibrium conditions, hence the aircraft is unable to control trimmed speed. The input is therefore completely ineffective to control trimmed flight conditions.

- (3) $\bar{x}_\alpha < \bar{x}_\delta < 0 \Rightarrow C_{L_\alpha}^{\text{tr}} < 0$ — If the CCoP falls fore of the neutral point but aft of the CG, the trimmed lift slope becomes negative. This means that an increase in trim lift coefficient must be achieved with a decrease in angle of attack. This counterintuitive behavior is explained by the significant control lift that must be generated to trim the aircraft with such a small moment arm, which requires a reduction in the lift of the bare airframe to maintain vertical equilibrium. This is still a rather inefficient use of the untrimmed $C_L(\alpha, \delta)$ range, as only a value much lower than the clean $C_{L_{\max}}$ can be reached in equilibrium flight with the available control authority. Furthermore, an increase in speed requires an increase in trim angle of attack. The inversion of this fundamental relation is potentially highly undesirable in operational practice, since α is related to θ , which is an intuitive visual cue for pilots.
- (4) $\bar{x}_\delta \rightarrow 0^\pm \Rightarrow C_{L_\alpha}^{\text{tr}} \rightarrow \pm\infty$ — If the CCoP falls in proximity of the CG, the trimmed lift slope diverges, making it possible to change trim lift coefficient at (almost) constant angle of attack. This is because the control device is capable to generate a trim pitching moment as a pure torque about the CG itself and its corresponding trim control lift changes linearly with the angle of attack as well. While this has the advantage of maintaining an almost fixed angle of attack margin before stall [27], it can also be rather undesirable since, once again, a large part of the lift carpet remain accessible only via values in α that cannot be achieved by means of δ in equilibrium flight.
- (5) $\bar{x}_\delta = 0 \Rightarrow C_{L_\alpha}^{\text{tr}} = 0$ — In the extreme case for which the CCoP coincides with the CG ($\bar{x}_\delta = 0$), the lift slope in trimmed flight is null, and the trim angle of attack is undefined. The aircraft can be trimmed at any angle of attack for a limited range of values of the desired trim lift coefficient. For the same reason, a change in airspeed requires no change in trim angle of attack, but only a change in the control input value that trims the aircraft in the new flight condition.
- (6) $\bar{x}_\delta > 0 \Rightarrow C_{L_\alpha}^{\text{tr}}/C_{L_\alpha} > 1$ — If the CCoP falls anywhere ahead of the CG, the trimmed lift slope is again positive and greater than the one of the bare airframe. In the particular case of the CCoP falling one static margin ahead of the CG ($\bar{x}_\delta = -\bar{x}_\alpha$), it is double. The control device increases the lifting capabilities of

the bare airframe in trim, and makes it possible to achieve the largest part of the available C_L range in equilibrium flight. In particular, equilibrium flight at a given angle of attack results in a higher lift coefficient than the one of the bare airframe, and the aircraft is able to make use of the entire C_L range efficiently. As for the conventional PAC case, an increase in speed requires an intuitive decrease in angle of attack to re-establish equilibrium flight conditions. This case is representative of aircraft equipped with over-the-wing-spoilers and/or canard wings.

A similar derivation for the lift slope in sustained maneuvering flight can be found in [1].

5. Control surface layouts

PAC impacts both the rotational and vertical dynamics of the aircraft, at the same time, by means of pitch moment generation. Because of this, controllability and dynamic stability are tightly connected [1]. This happens because the evolution of the flight path angle is intrinsically coupled to the evolution of the angle of attack of the airframe. Greater longitudinal stability results in stiffer transient response, smaller stability results in high agility, and instability results in a diverging trajectory to any longitudinal input.

The coupling between dynamic response and stability parameters — such as the static and maneuver margins — is already evident in simple relations as Eq. (29). These have been obtained by assuming that it is possible to reduce all control forces to one single location, which is fixed with respect to the airframe. So far, no attention has been put in the description of how such reduction process can be carried out.

When more control devices are available than those strictly necessary to control a given motion axis, they are said to be redundant. Redundant control devices can be linked together, and to the pilot input, in infinitely many different ways. The coordination of their deflection results in, among the other things, driving the location of the CCoP. If done according to a specific strategy, this can result in decoupling the stability and control characteristics of the aircraft to various extents. When these are perfectly uncoupled, the former only depend on the clean aerodynamics, mass and balance properties of the airframe, while the latter only depend on the FCS and control devices themselves. The possibility to install redundant control surfaces immediately raises important questions about control surface layouts and FCS design, coupling the aircraft design and control problems.

The following sections elaborate on the most fundamental relations between the CCoP, the control surface layout, and the architecture

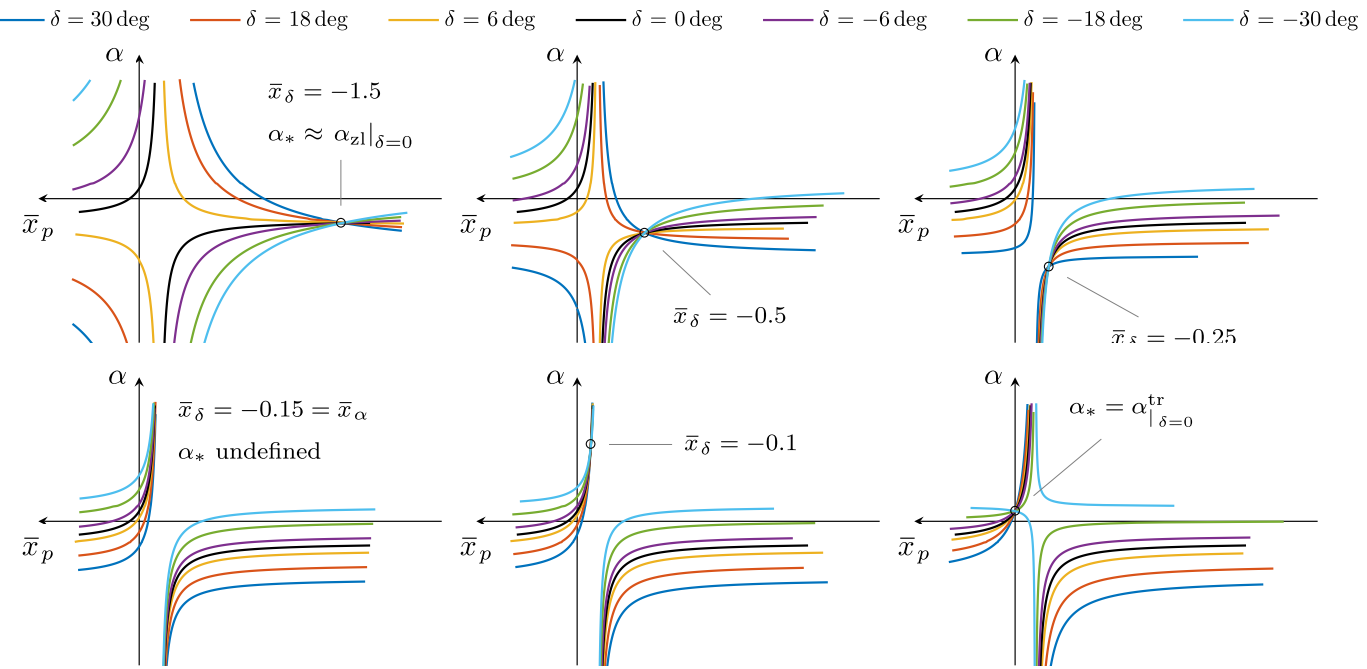


Fig. 13. Position of the Overall Center of Pressure (OCoP) as a function of the angle of attack, for different locations of the CCoP and control surface deflections. Linear aerodynamic model with one control surface, $C_{L_0} = 0.21$, $C_{L_a} = 0.119 \text{ deg}^{-1}$, $C_{M_0} = 0.015$, $\bar{x}_a = -0.15$, $\tau_\delta = -0.1$.

of the FCS, with primary focus on the role played by the number and location of available control surfaces. The discussion is structured around the DFPC possibilities enabled by an increasing number of (redundant) control surfaces, with particular focus on the first and foremost controllability requirement: trim. Additional relevant examples from more modern literature are also presented to elaborate on topics such as flying qualities, tracking precision and disturbance rejection for conventional and unconventional aircraft configurations which have not been covered in Section 3.

5.1. One control surface

In the case of only one movable surface dedicated to the control of the longitudinal axis, the CCoP has a fixed position which coincides with the location of the control surface itself. Starting from Eq. (30), a linear aerodynamic model with one movable surface can be expressed as in Eq. (46) [43].

$$\begin{cases} C_M(\alpha, \delta) = C_{M_0} + C_{M_a} \alpha + C_{M_\delta} \delta \\ C_L(\alpha, \delta) = C_{L_0} + C_{L_a} \alpha + C_{L_\delta} \delta \end{cases} \quad (46)$$

The corresponding ACoP can be expressed as in Eq. (47) starting from its definition in Eq. (31).

$$\bar{x}_p^A(\alpha) = \frac{C_{M_0} + C_{M_a} \alpha}{C_{L_0} + C_{L_a} \alpha} \quad (47)$$

The CCoP can be expressed as in Eq. (48) starting from its definition in Eq. (11) with $i = 1$, where x_1 is the location of the control surfaces and it can be assumed that $C_{M_\delta} \approx C_{L_\delta} \bar{x}_1$.

$$\bar{x}_\delta = \frac{C_{M_\delta} \delta}{C_{L_\delta} \delta} = \frac{C_{M_\delta}}{C_{L_\delta}} \approx \bar{x}_1 \quad (48)$$

The position of the OCoP is shown in Fig. 13 as a function of the angle of attack, for different locations of the control surface \bar{x}_δ and various control surface deflections.

The position of the CCoP is independent of the only control surface deflection, and it coincides with the ACoP, and therefore also with the OCoP, exclusively for one value of the angle of attack. This is reported in Eq. (49), obtained by equating Eqs. (47) and (48) and solving for α .

$$\alpha_* = \alpha_{z|_{\delta=0}} \frac{\bar{x}_\delta - \bar{x}_0}{\bar{x}_\delta - \bar{x}_a} \quad (49)$$

In this equation, $\alpha_{z|_{\delta=0}} = -C_{L_0}/C_{L_a}$ is the zero-lift angle of attack of the airframe, $\bar{x}_0 = C_{M_0}/C_{L_0}$ is the application point of the basic aerodynamic load, and $\bar{x}_a = C_{M_a}/C_{L_a}$ is the position of the neutral point. The corresponding lift and pitch coefficients are reported in Eqs. (50a) and (50b), respectively.

$$C_L^* = C_{L_0} \frac{\bar{x}_0 - \bar{x}_a}{\bar{x}_\delta - \bar{x}_a} + C_{L_\delta} \delta \quad (50a)$$

$$C_M^* = C_L^* \bar{x}_\delta \quad (50b)$$

It is evident that this angle of attack can be achieved in trimmed flight ($C_M^* = 0$) only when the total lift coefficient is zero ($C_L^* = 0$) or when the control surface is located at the aircraft CG ($\bar{x}_\delta = 0$). In the former case, the aircraft would be incapable to create net lift to sustain its weight. In the latter case, the value of the angle of attack for which the ACoP, the CCoP and the OCoP coincide — and also coincide with the CG — is given by Eq. (51).

$$\alpha_*^{\text{tr}} (\bar{x}_\delta = 0) = -\frac{C_{M_0}}{C_{M_a}} = \alpha_{z|_{\delta=0}}^{\text{tr}} \quad (51)$$

This is the trim angle of attack of the clean airframe, which indicates that such trim condition would be achieved when $\delta = 0$, and therefore the control surface would not be employed at all.

More generally, the angle of attack α^{tr} and control surface deflection δ^{tr} necessary to trim the aircraft and sustain its weight are uniquely determined by the two conditions $C_M(\alpha, \delta) = C_M^* = 0$ and $C_L(\alpha, \delta) = C_L^* \approx mg/q_\infty S$ to be imposed on Eq. (46). For given α^{tr} and δ^{tr} , the position of the OCoP is also uniquely determined, without any possibility to adjust it arbitrarily, as it can be seen by specializing its definition (Eq. (33)) to the case of trim with a single control surface (shown in Eq. (52)).

$$\bar{x}_p^{\text{tr}} = \bar{x}_p^A(\alpha^{\text{tr}}) + \frac{C_{L_\delta}}{C_L} \left[\bar{x}_\delta - \bar{x}_p^A(\alpha^{\text{tr}}) \right] \delta^{\text{tr}} \quad (52)$$

It can therefore be concluded that a single control surface is not sufficient to trim the aircraft in equilibrium flight and drive the position of the OCoP at the same time. Even in the special case for which the OCoP would be driven to coincide with the CCoP, the control surface would be ineffective. As a matter of fact, there are not enough control DoFs to fulfill the three desired objectives.

This simple derivation shows that at least two redundant control devices are necessary to control the airframe with desired characteristics of its response. In case only one control surface is available, its location is the only parameter that can be leveraged to achieve a desired position of the CCoP and hence shape the dynamic response of the airframe.

5.1.1. Impact of spoilers location on dynamic response

When only one control surface is dedicated to DLC, the aircraft transient response depends on the location of such control surface. Flight mechanics and control aspects become completely dependent on aircraft design.

The effect of the location of over-the-wing spoilers on the dynamic response of a light aircraft has been investigated in [47]. More than 100 piloted tests were carried out on a fixed-base modified Cessna Cardinal simulator to evaluate flight path control performance during landing maneuvers. Different groups of pilots were asked to land with and without the use of DLC spoilers, and to evaluate different input types and physical devices for deploying the spoilers. In all cases, maneuvers were carried out without an airspeed hold, which means without supporting the spoiler input with an automatic elevator deflection or throttle command. Spoilers were therefore the only devices dedicated to flight path control.

Different spoiler locations were simulated by assigning specified values to the pitch moment resulting from their deflection: the nominal location, one for Pure DLC, one for zero pitch moment, and one for constant lift coefficient. The latter was defined as to obtain the condition for which “the spoiler pitching moment caused the airplane to rotate to a higher angle of attack so that the increase in lift due to angle of attack equaled the loss in lift due to spoiler deflection” [47]. This is different from Pure DLC, for which the aircraft rotates to neutralize the total change in α (not C_L), and the total variation of C_L is equal to the increase due to control surfaces (confront Section 4).

Results showed that the initial altitude and load factor responses due to spoilers in the Pure DLC location were quickly neutralized by a variation in trim speed. The location for zero pitch moment resulted in small altitude variation, and excessive excitation of the phugoid mode. The nominal location and the one for constant lift coefficient were almost coincident, and resulted in the best handling qualities overall, with almost no variation in aircraft attitude and trimmed airspeed, and a satisfying altitude decrease. Conclusions state that DLC without automatic speed control is recommended only for incidental maneuvers, especially during descent and landing phases, as the airplane responds to variations in C_L with variations in V . If an airspeed hold is not available, spoilers located where their deflection guarantees constant C_L obtain the best handling qualities for flight path control. Consequently, the term DLC is suggested to be inappropriate for this particular application, and the term “Descent Rate Control” is proposed.

5.2. Two control surfaces

It has just been shown that, when only one control surface is dedicated to longitudinal control, the position of the CCoP coincides with the control surface itself, and is therefore fixed. For a given control input, the dynamic response of the aircraft is only dependent on airframe design parameters, and cannot be adapted to different tasks using the same control surface.

Two redundant control surfaces at different longitudinal positions x_1 and x_2 can be coordinated in different ways according to necessity. In modern FCSs, this would be typically done with FBW systems. In the most simple implementation, they could be ganged together so that their coordinated deflections result in a specific position of the CCoP [1]. Together with the angle of attack, the two deflections would provide — in principle — just enough DoFs to trim the aircraft for vertical and rotational equilibrium, and assign a desired position to the

CCoP. For a given airframe design, the gearing ratio can be selected to achieve desired characteristics of the transient response of the aircraft.

This is shown by expanding the generic linear aerodynamic model of Eq. (46) to include two movable surfaces, as reported in Eq. (53).

$$\begin{cases} C_M(\alpha, \delta_1, \delta_2) = C_{M_0} + C_{M_\alpha} \alpha + C_{M_{\delta_1}} \delta_1 + C_{M_{\delta_2}} \delta_2 \\ C_L(\alpha, \delta_1, \delta_2) = C_{L_0} + C_{L_\alpha} \alpha + C_{L_{\delta_1}} \delta_1 + C_{L_{\delta_2}} \delta_2 \end{cases} \quad (53)$$

The CCoP can be calculated as in Eq. (54) starting from its definition (Eq. (11) with $i = 2$).

$$\bar{x}_\delta(\delta_1, \delta_2) = \frac{C_{M_{\delta_1}} \delta_1 + C_{M_{\delta_2}} \delta_2}{C_{L_{\delta_1}} \delta_1 + C_{L_{\delta_2}} \delta_2} \approx \frac{C_{L_{\delta_1}} \bar{x}_1 \delta_1 + C_{L_{\delta_2}} \bar{x}_2 \delta_2}{C_{L_{\delta_1}} \delta_1 + C_{L_{\delta_2}} \delta_2} \quad (54)$$

If a reference position of the CCoP is desired, the latter relation can be solved for the ganging ratio G_{21} between the two control surface deflections, as shown in Eq. (55).

$$G_{21} = \frac{\delta_2}{\delta_1} = \frac{C_{M_{\delta_1}} - C_{L_{\delta_1}} \bar{x}_\delta}{C_{L_{\delta_2}} \bar{x}_\delta - C_{M_{\delta_2}}} \approx \frac{C_{L_{\delta_1}} (\bar{x}_\delta - \bar{x}_1)}{C_{L_{\delta_2}} (\bar{x}_2 - \bar{x}_\delta)} \quad (55)$$

The angle of attack α^{tr} and control surface deflections δ_1^{tr} and δ_2^{tr} necessary to achieve trimmed flight while maintaining an assigned position of the CCoP are obtained by imposing the conditions $C_M(\alpha, \delta_1, \delta_2) = C_M^{\text{tr}} = 0$ and $C_L(\alpha, \delta_1, \delta_2) = C_L^{\text{tr}} \approx mg/q_\infty S$ on Eq. (53) while using Eq. (55) to constrain the relative deflection of the two movable surfaces. This results in a system of three equations in three unknowns, whose solution is reported in the following Eqs. (56a)–(56c),

$$\alpha^{\text{tr}} = \alpha^{\text{tr}}|_{\delta_{1,2}=0} - \frac{\bar{x}_\delta}{1 - \bar{x}_\delta} \Delta C_L^{\text{tr}} \quad (56a)$$

$$\delta_1^{\text{tr}} = \frac{\Delta C_L^{\text{tr}}}{C_{L_{\delta_1}}} \cdot \frac{\bar{x}_2 - \bar{x}_\delta}{(\bar{x}_2 - \bar{x}_1)(1 - \bar{x}_\delta)} \quad (56b)$$

$$\delta_2^{\text{tr}} = G_{21} \delta_1^{\text{tr}} = \frac{\Delta C_L^{\text{tr}}}{C_{L_{\delta_2}}} \cdot \frac{\bar{x}_\delta - \bar{x}_1}{(\bar{x}_2 - \bar{x}_1)(1 - \bar{x}_\delta)} \quad (56c)$$

where

$$\Delta C_L^{\text{tr}} = C_L^{\text{tr}} - C_{L_0} - C_{L_\alpha}|_{\delta_{1,2}=0} \quad (57a)$$

$$\alpha^{\text{tr}}|_{\delta_{1,2}=0} = -C_{M_0}/C_{M_\alpha} \quad (57b)$$

For any given value of C_L^{tr} , the angle of attack required for trim does not depend on the position of either control surface, but rather on the position of the CCoP. It diverges for $\bar{x}_\delta \rightarrow 1$ and, away from this condition, it rapidly settles on the value of the trim angle of the clean airframe $\alpha^{\text{tr}}|_{\delta_{1,2}=0}$ as shown in Fig. 14. Because both trim deflections are also diverging for $\bar{x}_\delta = 1$, trim cannot be maintained in this condition. For a given C_L^{tr} and \bar{x}_δ , both trim deflections decrease in magnitude if the two control surfaces are installed far away from each other ($|\bar{x}_2 - \bar{x}_1| \gg 0$), as shown in Fig. 15. The required trim deflection of one control surface is null if the position of the CCoP has to coincide with the other control surface. On the other hand, the closer a control surface is placed to $\bar{x} = 1$, the weaker the influence of \bar{x}_δ is on the trim deflection of the other control surface. If $\bar{x}_1 = 1$, for instance, δ_2^{tr} is completely independent of the position of the CCoP, as shown in the last row of Fig. 15.

The last observation prompts to investigate the possibility of employing one control surface, independently from the other and in combination with the angle of attack, to trim the aircraft for pitch and vertical equilibrium, while dedicating the other control surface to DFPC. The latter would have to be located fore of the aircraft CG, by a distance approximately equal to the mean aerodynamic chord. This scenario resembles the most common use of tail elevators and over-the-wing spoilers in current commercial aircraft operations. The same considerations made in the previous Section 5.1 would then hold.

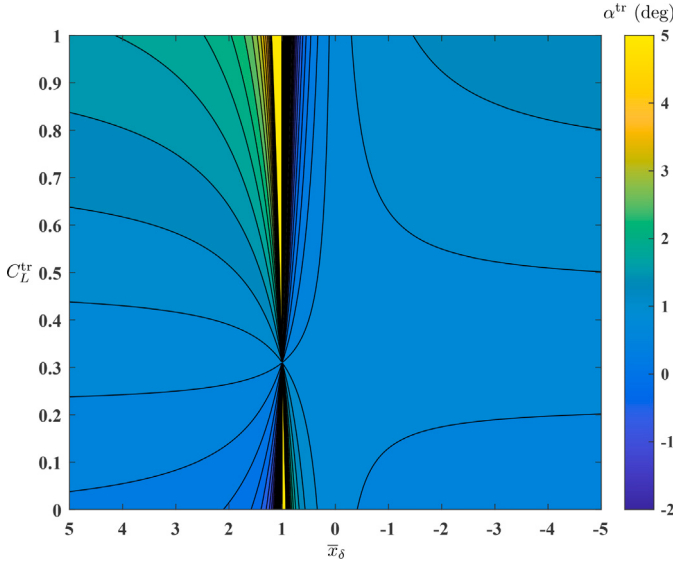


Fig. 14. Contour plot of α^{tr} for different values of \bar{x}_δ and C_L^{tr} , with $C_{L_0} = 0.21$, $C_{L_a} = 0.119/\text{deg}$, and $\alpha_{|_{\delta_{1,2}=0}}^{\text{tr}} = 0.84 \text{ deg}$.

5.2.1. Flying qualities and tracking precision

If the trailing-edge flaps (or the over-the-wing spoilers) on the main wing are ganged together to move symmetrically, they act as a single control surface which can be coordinated with the tail elevator to achieve DFPC. This is by far the most common scenario found in engineering applications.

A ganging ratio as the one introduced in Eq. (55) is the starting point in [48] to allow various forms of DFPC on conventional aircraft architectures. The resulting mechanical linkage is represented in Fig. 16. An additional control law is designed with a high-pass filter and cross-connection between the two control surfaces. Classic flying qualities such as the stick displacement per g , the Control Anticipation Parameter, and the Transient Response criterion C^* are evaluated as a function of various FCS parameters.

A similar evaluation is done for newly proposed flying qualities criteria, originally defined with the purpose to measure the ability to achieve a DLC motion type. These are, namely:

- a DLC efficiency coefficient, defined as the ratio between the initial and steady-state values of the load factor response to a longitudinal step input;
- a metric to quantify the increase in rate of climb, defined as the change in steady rate of climb obtained by using DLC as compared to when not using it, normalized by the steady-state load factor after a step longitudinal input;
- a normalized alternative to the previous one, defined as the ratio between the rate of climb obtained with DLC and the one obtainable in the case of constant vertical acceleration.

Simulation results are presented for linearized models of a Douglas A-4 Skyhawk military jet aircraft and a PZL-Mielec M-18 Dromader agricultural aircraft.

In [49], a linear control law is designed to improve the path tracking precision of a Piper PA18 Super Club aircraft. It achieves great performance in terms of accuracy and robustness thanks to the combined implementation of an inner loop based on body acceleration measurements and DLC. The latter is achieved by coupling trailing-edge control surfaces on the main wing with the tail elevator through an angle of attack set-point. Flaps and ailerons are used as the main control surface dedicated to DLC, while the elevator is used to prevent stall and washout the flaps deflection.

A similar approach is adopted in [15] by integrating DLC in the non-linear control law of the VFW-614-based ATTAS laboratory aircraft of DLR. Results show that this implementation of DLC allows to control lift independently from aircraft attitude, and increases the bandwidth of the vertical axis controller by more than 100%. This is discussed more extensively in Section 6.

5.3. Multiple redundant control surfaces

The linear aerodynamic model used in previous sections can be generalized as in Eq. (58a), and the CCoP can be calculated as in Eq. (58b).

$$\left\{ \begin{array}{l} C_M(\alpha, \delta_i) = C_{M_0} + C_{M_\alpha} \alpha + \sum_{i=1}^n C_{M_{\delta_i}} \delta_i \\ C_L(\alpha, \delta_i) = C_{L_0} + C_{L_\alpha} \alpha + \sum_{i=1}^n C_{L_{\delta_i}} \delta_i \end{array} \right. \quad (58a)$$

$$\bar{x}_\delta(\alpha, \delta_i) = \frac{\sum_{i=1}^n C_{M_{\delta_i}} \delta_i}{\sum_{i=1}^n C_{L_{\delta_i}} \delta_i} \approx \frac{\sum_{i=1}^n C_{L_{\delta_i}} \bar{x}_i \delta_i}{\sum_{i=1}^n C_{L_{\delta_i}} \delta_i} \quad (58b)$$

The latter expression, can be represented in matrix form as in the following Eq. (59),

$$\bar{x}_\delta = \frac{B_M \delta}{B_L \delta} \approx \frac{B_L X \delta}{B_L \delta} \quad (59)$$

where B_M and B_L are the row vectors of pitch and lift control effectiveness of all control surfaces, and X is the diagonal matrix of control surface locations \bar{x}_i . Coordinating the deflection of all redundant control surfaces to achieve a desired position of the CCoP translates then to solving the following Eq. (60) for δ .

$$\sum_{i=1}^n C_{L_{\delta_i}} (\bar{x}_i - \bar{x}_\delta) \delta_i = B_L (X - \bar{x}_\delta) \delta = 0, \quad \text{with } \delta \neq 0 \quad (60)$$

Together with a constraint on vertical equilibrium and one for trimming the pitch moment, Eq. (60) forms a system of three equations in $n+1$ unknowns, including control surface deflections and the angle of attack. When more than two control surfaces are redundant on the longitudinal axis of the aircraft, the possibilities to coordinate their deflections — together with α — are infinite, and the problem of achieving trimmed vertical equilibrium with a desired position of the CCoP is under-determined. This situation allows vast freedom in the design of the control surface layout and in the implementation of the FCS, which could be exploited to achieve optimum desired performance according to different criteria.

One generic, flexible approach that allows to calculate the combination of control surface deflections required to perform a given task is represented by Control Allocation (CA) methods [50]. The baseline CA problem consists in finding the value of δ which solves the following Eq. (61).

$$\nu \approx B_\nu \delta = B_\nu G \epsilon, \quad \text{with } B_\nu = \frac{\partial \nu}{\partial \delta} \quad (61)$$

Here, ν is an array of control objectives — in the most common “three moment problem”, these are the three control moments C_L , C_M , C_N or the angular rates p , q , r — prescribed by the pilot or control law, and B_ν is the control effectiveness matrix that maps control surface deflections to such objectives. G is a ganging matrix which optionally constrains the relative deflection of the actual control surfaces δ , resulting in the creation of a smaller set of “virtual” control surfaces ϵ , such that $\delta = G\epsilon$.

If the number of (virtual) control surfaces is larger than the number of control objectives, the B_ν matrix (or its virtual equivalent $B_\nu G$) is not square and cannot be inverted. CA methods define an analytic or algorithmic function f_{CA} that calculates the optimal control surface deflections δ to obtain the required control objectives ν , on the basis of the available effectiveness B_ν and, optionally, other flight or design parameters — such as control surface saturation limits, for example.

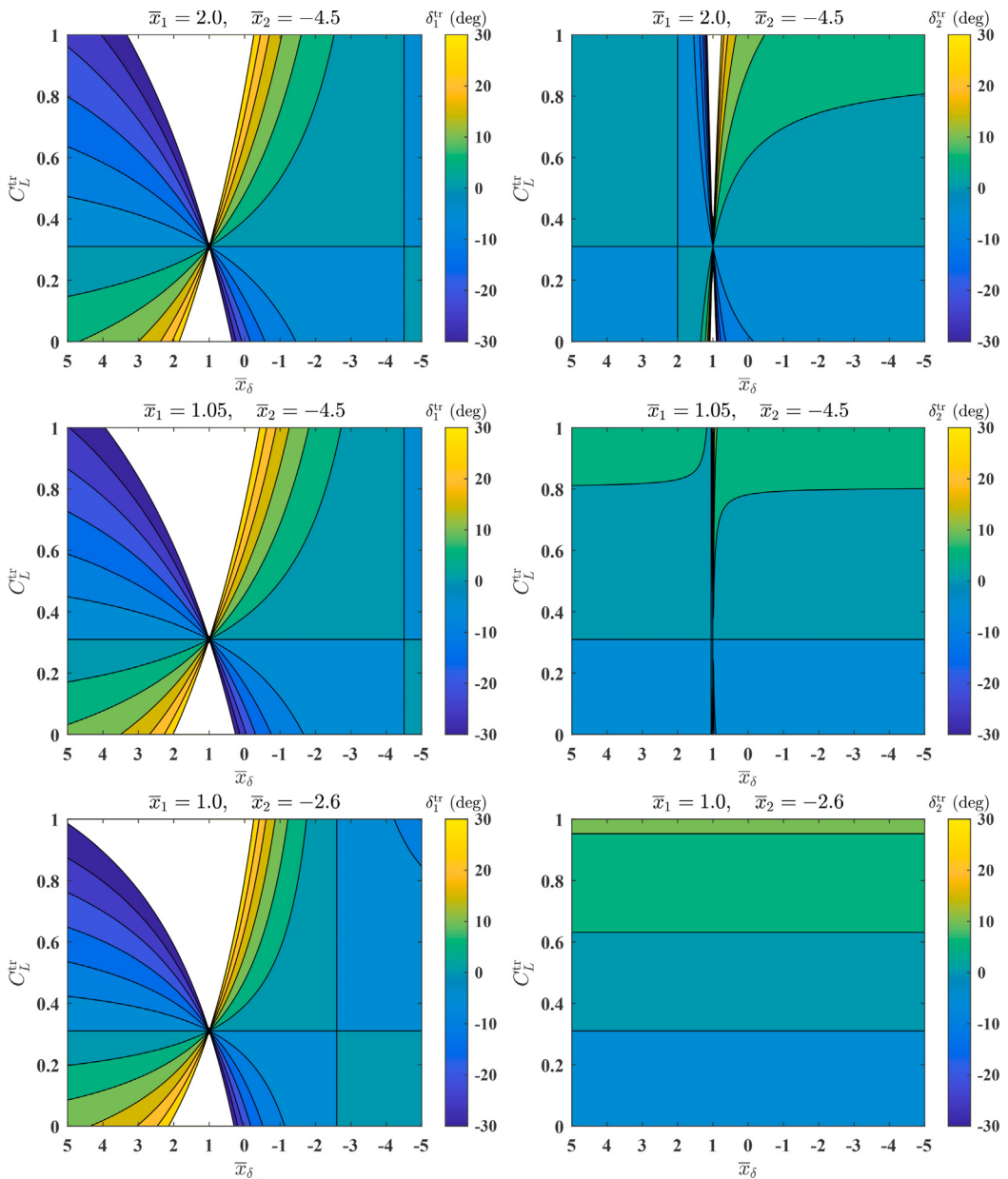


Fig. 15. Contour plot of δ_1^{tr} and δ_2^{tr} for different values of \bar{x}_δ and C_L^{tr} , with $C_{L_{\delta_1}} = 0.012/\text{deg}$, $C_{L_{\delta_2}} = 0.018/\text{deg}$, \bar{x}_1 and \bar{x}_2 indicated on top of each chart, and other parameters as in Fig. 14. The white areas are unattainable due to control surface saturation limits, as indicated in the color bars.

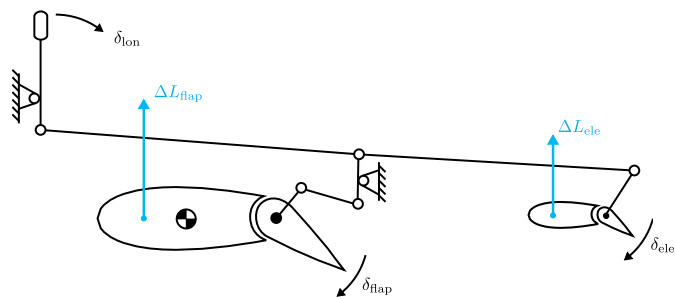


Fig. 16. Mechanical linkage between the pilot command stick, the front flap and the tail elevator to achieve DLC of conventional aircraft configurations.

Source: Adapted from [48].

The generic solution to the CA problem may be expressed as in Eq. (62).

$$\delta = f_{\text{CA}}(B_v, v, \dots) \quad (62)$$

A vast variety of CA methods is available in scientific literature. Most of them rise from the formulation of an optimization problem to be solved online, but may differ in both the main idea behind the approach, and the algorithm to implement it. A broad and detailed survey of CA approaches, algorithms and applications is presented in [51] for both linear and non-linear physical models, and not only pertaining to the field of aeronautics. A survey and evaluation of optimization methods for the most classic approaches is provided in [52].

5.3.1. Flight mechanics of staggered box-wing aircraft

Despite the countless developments that CA theory has enjoyed in the past two decades, only a few efforts have been dedicated to employing CA methods to the explicit achievement of DLC. A reason could lie in the fact that the possibility to implement DLC is not only dependent on the capabilities of the FCS, but also — and more

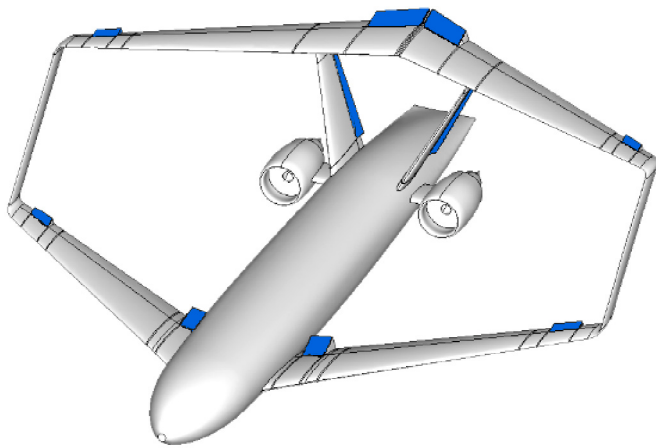
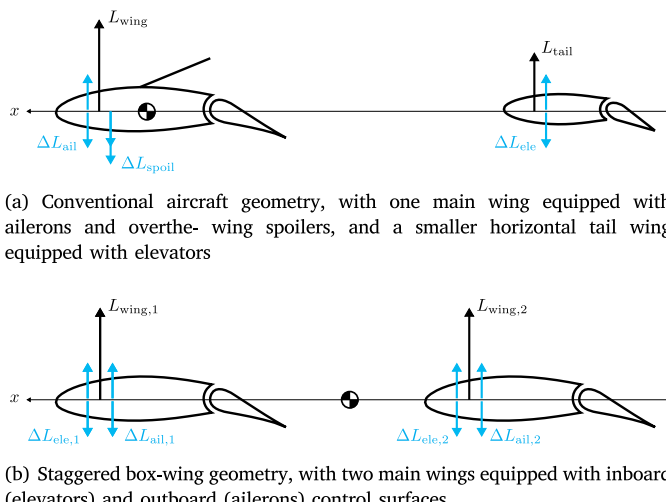


Fig. 17. Staggered box-wing aircraft with redundant control surfaces [54].



(a) Conventional aircraft geometry, with one main wing equipped with ailerons and over-the-wing spoilers, and a smaller horizontal tail wing equipped with elevators

(b) Staggered box-wing geometry, with two main wings equipped with inboard (elevators) and outboard (aileron) control surfaces

Fig. 18. Lift forces generated by wings and control surfaces, for a conventional and a staggered box-wing configuration [5].

fundamentally — on the geometry of the aircraft configuration, and not all aircraft configurations are capable of achieving DLC.

Multi-wing and box-wing aircraft with staggered lifting surfaces can accommodate the installation of redundant primary control surfaces at different longitudinal positions. These can enable innovative ways of controlling the position of the CCoP and achieving DLC, if coordinated through appropriate control laws. A staggered box-wing aircraft referred to as the “Prandtlplane” is presented in [53], with exemplary control surfaces layouts featuring two or four control surfaces per wing, both fore and aft the CG, as shown in Fig. 17. Its geometry introduces innovative ways to exploit various levels of control surface redundancy, making it the ideal platform to explore DFPC and DLC capabilities [5]. A synthetic representation of the main control forces in play along the vertical axis is represented in the free-body diagrams of Fig. 18, together with a comparison with the case of a conventional aircraft configuration.

An early demonstration of the capability of this aircraft to achieve both PAC and DLC motion types is reported in [55]. A more recent study proposes two CA formulations which are capable of shaping the dynamic transient response of an aircraft by inducing a preferred position of the CCoP [54]. By using the longitudinal position of the CCoP as a top-level input for the FCS, the study shows how generic CA methods can be tailored to achieve transient response characteristics

that are typical of DLC or PAC. The first formulation is based on the straightforward augmentation of the control effectiveness matrix B_v using the general definition of the CCoP (Eq. (58b)). It can be fed to any type of numerical algorithm, but incurs in an ill-conditioned B_v matrix when the desired position of the CCoP approaches the aircraft CG. The second formulation leverages a classic CA method based on generalized inverse matrices, and uses the desired position of the CCoP to weigh and prioritize the available redundant control surface deflections.

Several flight simulations show how DLC — and DFPC, in general — achieve better performance in terms of flight path tracking precision and disturbance rejection when performing fast, sharp maneuvers in classic flight scenarios including turbulent atmosphere [5]. An example of these is shown in Fig. 19. From the same time histories, a frequency-weighted measure of the Root Mean Square (RMS) acceleration at the aircraft CG was used to conclude that the location of the CCoP, and hence the type of DFPC achieved, have a significant impact on the comfort perceived on-board (Fig. 20) [5].

For the same staggered box-wing geometry, a methodology is developed in [57] to exploit the redundancy of control surfaces to trim the aircraft for maximum control authority about specified motion axes. Results are provided for trimmed flight with 3 and 6 DoFs, and compare a classic “three moment” CA problem formulation with a four-objective CA problem including the explicit allocation of the lift force achievable by control surfaces. They show how the control surface layout allowed by the staggered box-wing makes it possible to seamlessly trade α -generated lift with control lift due control surface deflections. This flexibility makes it possible for such aircraft to achieve widely different trim conditions, evident in Fig. 21, and depending on the specified objective function.

Other notable attempts at including direct force control in the CA problem formulation revolve around online drag minimization [58,59], while the earliest attempts to solve CA problems with four or more objectives are presented in [60].

6. Inflight demonstration

On the now retired VFW-614-based ATTAS laboratory aircraft of DLR — introduced in Section 3.3 — capabilities for DLC were included primarily for the purpose of inflight simulation. However, they also provided an opportunity for research on flight control and guidance algorithms, as described in previous research featuring inflight experiments [15]. The main contribution of that research line lied in the way DLC and attitude control laws were integrated, and is described subsequently.

In that context, a set of nonlinear auto-flight control laws incorporating DLC was designed and flight-tested on ATTAS. This was an extension of a previously developed set of nonlinear flight control laws [61]. This control setup was augmented for flight path control by making use of specially designed DLC flaps on ATTAS. Such augmentation served a double purpose. Firstly, aircraft responses to flight path angle commands were made faster and more accurate. Secondly, turbulence induced disturbances were rejected to improve passenger comfort.

This section shows the integration of DLC in nonlinear auto-flight control laws, and the achieved results obtained through computer simulation and flight demonstration.

6.1. Flight control law architecture

The auto-FCS consists of three consecutive Non-linear Dynamic Inversion (NDI) loops, relying on the concept of time scale separation. Each loop consists of an NDI control law (including CA), a first- or second-order linear controller, and a first-order reference model [15,61,62]. Such baseline architecture is illustrated in Fig. 22, while a top-level overview of the control law is shown Fig. 23.

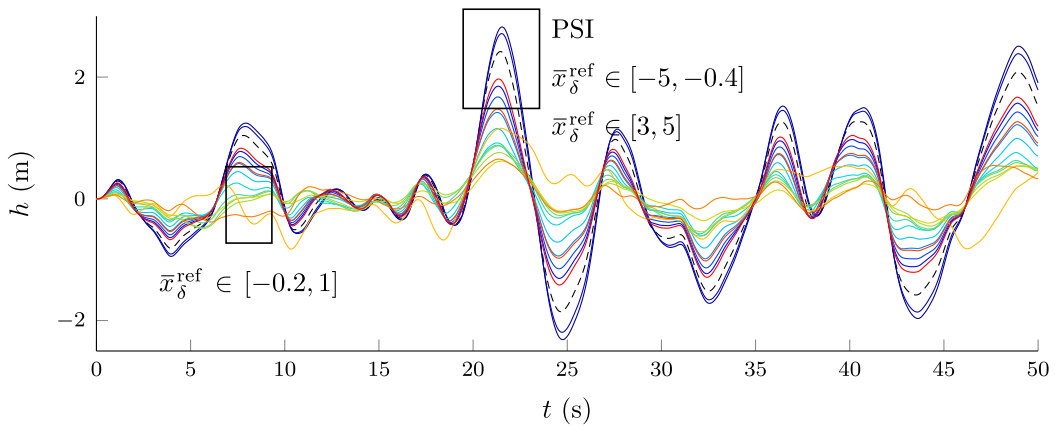


Fig. 19. Altitude time histories of an altitude-hold task in turbulent atmosphere, for a novel CA method prescribing different values of the CCoP location $\bar{x}_{\delta}^{\text{ref}}$ and the standard Pseudo Inverse (PSI) method [54].

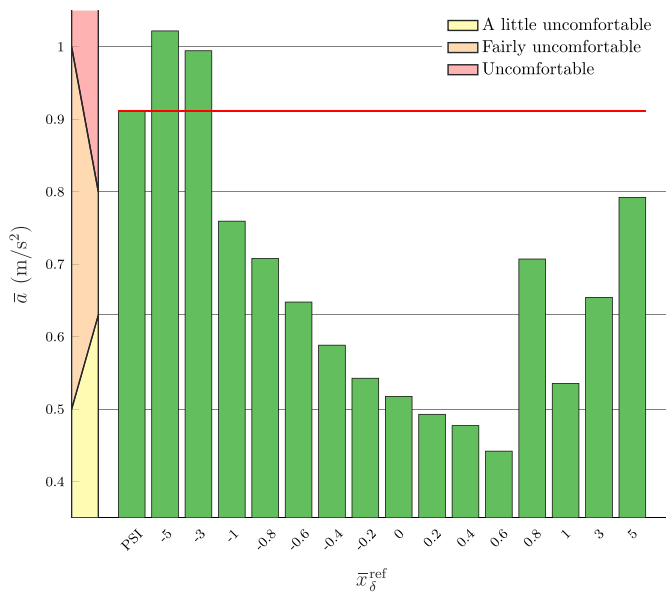


Fig. 20. Overall frequency weighted RMS acceleration perceived at the aircraft CG and corresponding perceived comfort level for a novel CA method prescribing different values of the CCoP location $\bar{x}_{\delta}^{\text{ref}}$ and the standard Pseudo Inverse (PSI) method, during the same altitude-hold task referred to in Fig. 19 [54,56].

NDI allows to cancel out the nonlinear aircraft dynamics such that the resulting closed-loop system behaves like a single pure r th order integrator. For a first-order Multi-Input Multi-Output (MIMO) dynamic system model which can be assumed to be affine in the input u , this is achieved by introducing a virtual outer loop control input vector v , as shown in (63), where $f(\hat{x}, \hat{p})$ represents the estimated airframe/engine model and $G(\hat{x}, \hat{p})$ is the estimated effector blending model, which needs to be inverted.

$$\dot{x} = f(x, p) + G(x, p)u \quad (63a)$$

$$u = G^{-1}(\hat{x}, \hat{p}) [v - f(\hat{x}, \hat{p})] \quad (63b)$$

Main advantages of NDI consist in decoupling control of different motion axes, as well as removing the need for gain scheduling of the outer loop linear controller. In this way, a simple linear controller as outer loop can achieve desired stability and performance of the overall controlled system. Despite this particular approach is not perfect due to the presence of the multiplicative uncertainties in the aerodynamic

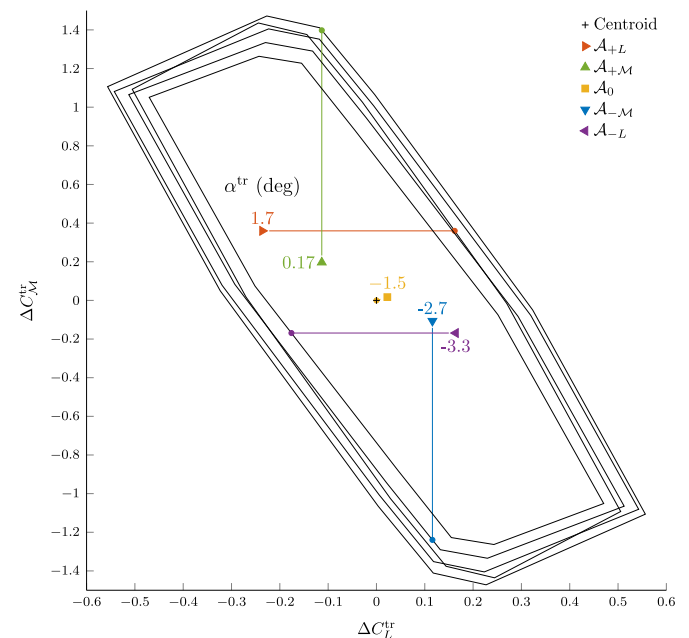


Fig. 21. Trim conditions maximizing control authorities \mathcal{A} about different directions on the pitch and lift axes, for $V^{\text{tr}} = 180 \text{ m/s}$ [57].

model, the linear controller has shown in past applications to be capable to deal satisfactorily with such modeling errors [63,64]. However, special protections are needed to prevent control input saturation [65].

The dynamic part of the FCS complies with the principle of time scale separation, as the aerodynamic moments have typically a higher bandwidth than the aerodynamic forces. Since the DLC flaps have a direct influence on the lift force, without non-minimum phase transient, they can improve the agility of the aircraft. They have therefore a complementary nature with respect to the elevator.

The DLC flaps of the ATTAS are operational in flight conditions with flap settings 1, 5, and 14. Their nonlinear influence on C_L is illustrated in Fig. 24, and can be described by the third order polynomial relation of Eq. (64) [66].

$$\Delta C_{\text{DLC}} = 2(L_1 \delta_{\text{DLC}} + L_2 \delta_{\text{DLC}}^2 + L_3 \delta_{\text{DLC}}^3) \quad (64)$$

In the FCS, this relation has been implemented by means of a look-up table that maps DLC deflection between -30 deg and 20 deg to their DLC lift force contribution. Inverse table look-up is allowed to extrapolate, but the computed control deflections are then clipped to

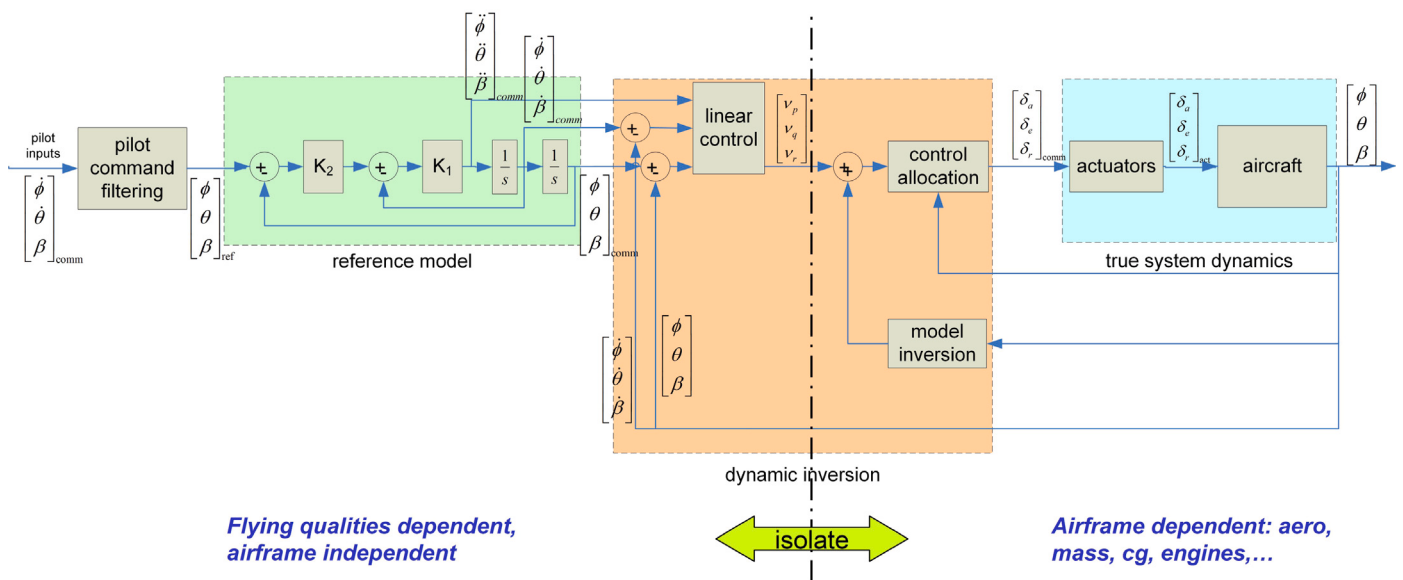


Fig. 22. Baseline architecture of an NDI loop with an outer linear controller.

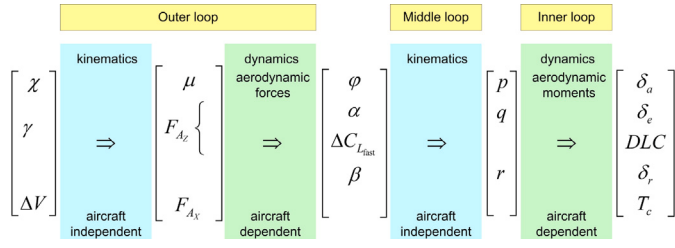


Fig. 23. Top-level overview of the auto-FCS architecture based on time scale separation, including DLC.

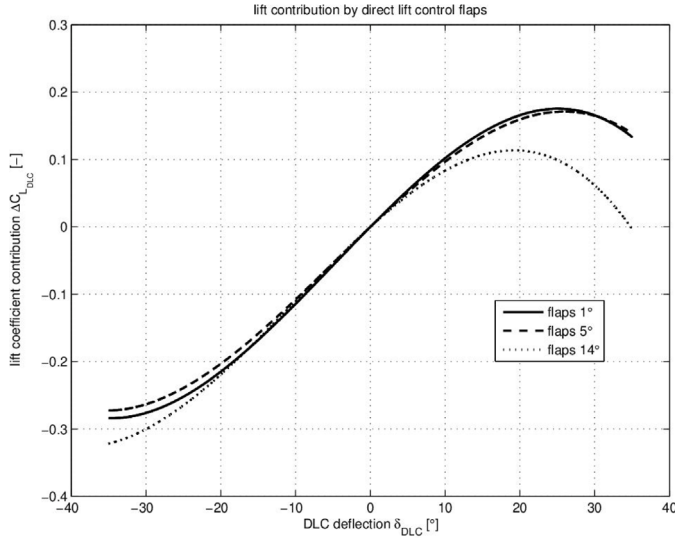


Fig. 24. Lift contribution of DLC flaps of the ATTAS inflight simulator.

the aforementioned saturation limits.

The NDI-based auto-FCS calculates the angle of attack α and DLC flap deflection δ_{DLC} required to generate a prescribed aerodynamic force F_{A_z} . The C_L contribution that must be provided by the DLC flaps is calculated as in Eq. (65), where α_m is the measured angle of attack,

and α_{comm} is the commanded one, obtained by inverting the airframe dynamics according to Eq. (63b).

$$\Delta C_{L_{DLC,comm}} = C_{L_\alpha} (\alpha_{comm} - \alpha_m) \quad (65)$$

The corresponding flap deflection is calculated by means of the look-up table mentioned earlier.

Since the reference model for the angle of attack is in fact a first-order filter, α_{comm} is actually low-pass filtered while being processed through the α reference model. DLC is included in the FCS architecture as a parallel ‘‘bypass’’ path going straight from the vertical aerodynamic force F_{A_z} towards the control effectors δ_{DLC} , as shown in Fig. 25. Since DLC acts complementary to the slower angle of attack (because of the low pass filtering in the reference model), its behavior has in fact washout characteristics. Adding DLC increases significantly the bandwidth of the γ channel, as demonstrated by the experimental results presented in the following sections.

6.2. Computer simulations

Computer simulations demonstrate the beneficial influence of DLC on tracking performance as well as on rejection of atmospheric disturbance.

6.2.1. Tracking performance of DLC

A change in flight path angle $\Delta\gamma = 3$ deg has been commanded with and without DLC. Results of the arising dynamic evolution are shown in Fig. 26.

The flight path angle response without DLC is reported in Fig. 26(a). In this case, the change in γ is achieved by the elevator only. A time delay in the response of γ can be seen, as well as a small opposite initial response representative of a non-minimum phase behavior. The reason for this is explained with the help of the related free-body diagram. The elevator deflects upwards ($\delta_e < 0$ in Fig. 26(a)), which causes an instantaneous brief decrease in total lift on the aircraft ($\Delta L_{tail} < 0$). Simultaneously, a pitch-up moment $M > 0$ is generated, which sets off a sequence of positive pitch rate $q > 0$, positive change in angle of attack $\Delta\alpha > 0$, positive lift change $\Delta L > 0$ and thus a climbing flight path angle $\gamma > 0$. Due to the principle of time scale separation, which should be evident also from Fig. 23, this sequence results in a time delay.

The flight path response with DLC is reported in Fig. 26(b). In this case, the change in γ is achieved by cooperating elevator and DLC

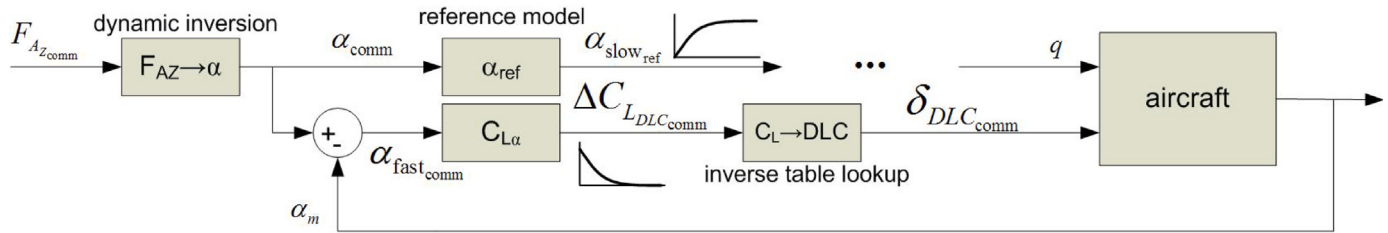


Fig. 25. Frequency-based distribution of commanded vertical aerodynamic force $F_{A_z,comm}$ over slower reference angle of attack $\alpha_{slow,ref}$ and faster DLC flap deflection $\delta_{DLC,comm}$.

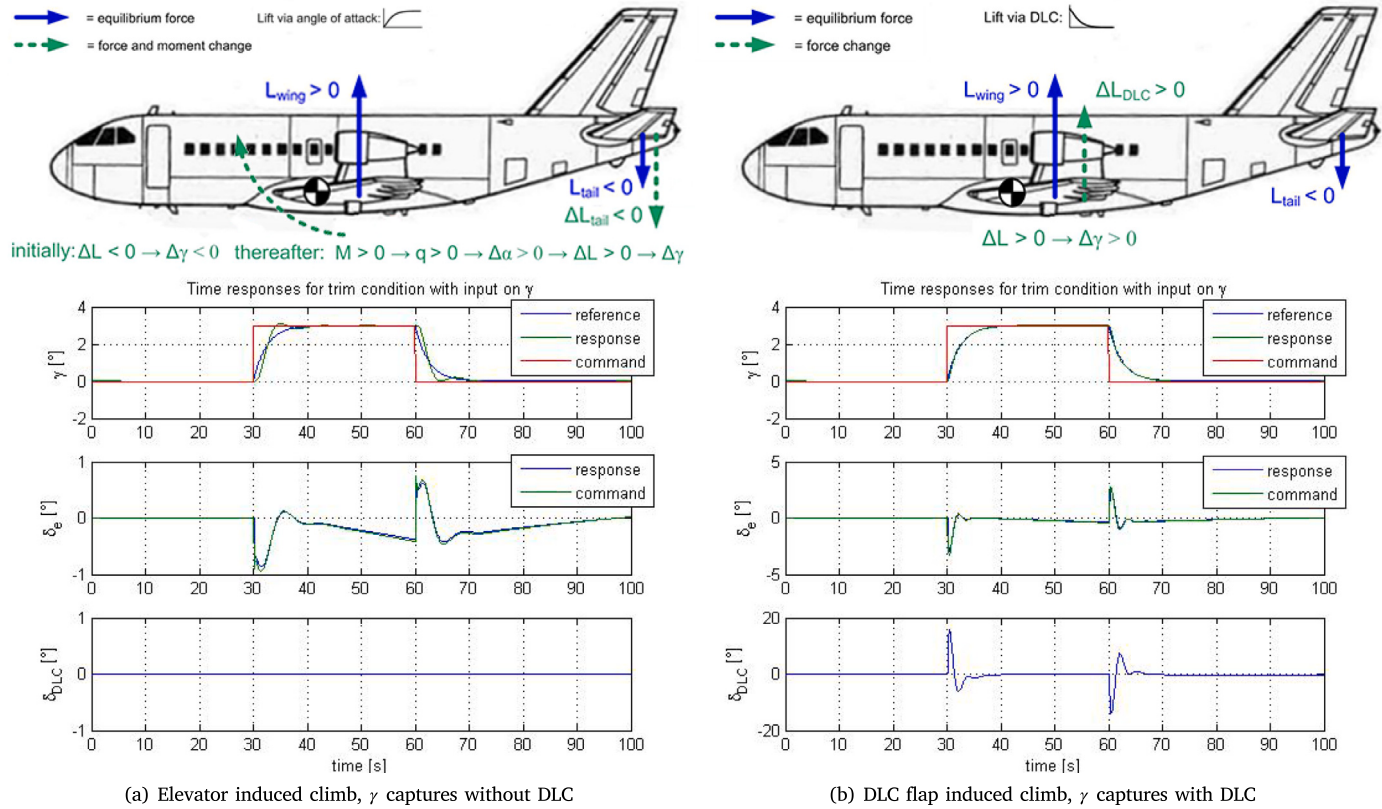


Fig. 26. Comparison of time responses of flight path angle captures with and without DLC, with related free-body diagrams.

flaps. In the related free-body diagram, the downward deflection of the DLC flaps ($\delta_{DLC} > 0$ in Fig. 26(b)) has a direct influence on the total lift of the aircraft $\Delta L > 0$, and thus generates a climbing flight path angle $\gamma > 0$ without time delay and without pitch moment. The dynamic response tracks the reference signal γ_{ref} very accurately. The DLC flaps have only an intermediate, short-term "washout" influence to eliminate the non-minimum phase behavior and related time delay of the elevator. While they act complementarily to the elevator action, which takes some time to build up a change in γ , the latter is still dominant in the longer term, as also shown in Fig. 27.

6.2.2. Turbulence disturbance rejection of DLC

Since DLC reacts faster on tracking errors, it can also contribute beneficially with respect to rejection of atmospheric disturbance, such as gusts or turbulent fields. Two simulation runs have been made for level flight through the same turbulence profile, with and without DLC. A reference flight path angle $\gamma_{ref} = 0$ was being tracked. Fig. 28 compares the time histories of flight path angle γ and pitch attitude angle θ during these 80 s simulation runs. From the figure, it can be seen that the time responses have in general smaller turbulence induced peaks, thanks to DLC. This confirms that DLC effectively reduces turbulence

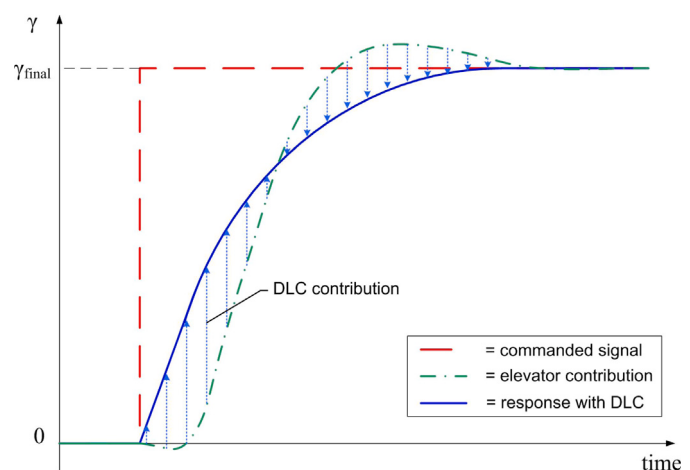


Fig. 27. Elevator and DLC contributions in response to a step change in the reference flight path angle γ .

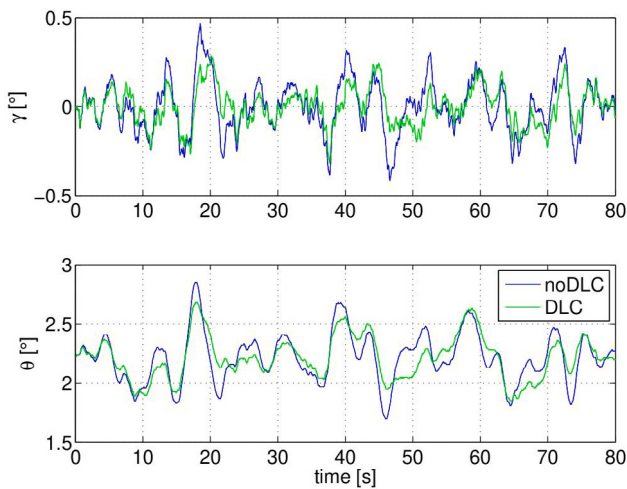


Fig. 28. Time histories of the flight path angle γ and pitch angle θ during a flight path hold task to evaluate turbulence rejection performance. Comparison between control with and without DLC.

induced disturbances and, as such, can result in increased passenger comfort on board.

6.3. Flight tests

On November 3rd 2011, a flight test with ATTAS was performed to evaluate the performance of the nonlinear auto-FCS in a realistic environment. The experimental procedure and the final results are presented in this section.

6.3.1. Experimental procedure

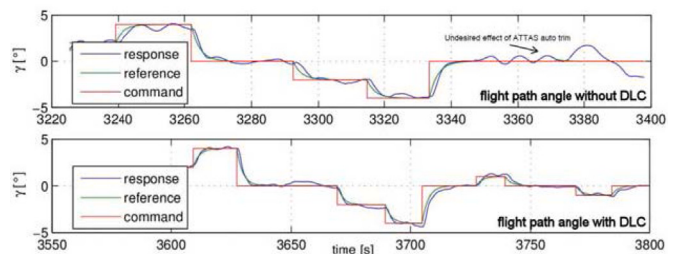
The experiments related to DLC have been performed in the following flight condition: altitude was about 1500 ft, Indicated Airspeed (IAS) was 180 kts with $\delta_{\text{flap}} = 1$ deg, landing gear and over-the-wing spoilers were retracted. Auto-trim and auto-throttle were both active during the tests.

During the experiments, the evaluation pilot executed various flight path angle captures in order to verify the performance of the tracking mode with and without DLC [61]. These captures were initiated by the evaluation pilot through the mode control panel. In order to obtain pure step commands, an activation switch was incorporated. This needed to be pressed after a desired value for the change in flight path angle had been dialed. Performance related to atmospheric disturbance rejection could not be verified during the test flight, since no turbulence was encountered.

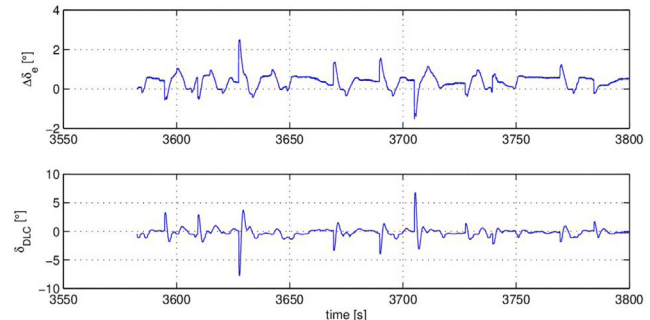
6.3.2. Experimental results

Time histories of the flight path angle captures are compared in Fig. 29(a) for the two cases, with and without DLC. The oscillating behavior of the flight path angle after each capture is caused by the perturbing auto-trim actions. From the charts, it can be deduced that DLC assists in tracking the reference flight path angle γ_{ref} more accurately.

Time histories of the elevator and DLC flap deflections are reported in Fig. 29(b) for the case when DLC was active. A comparison between the two charts reveals opposite motion of these control surfaces. This is because the flaps have a direct influence on the lift force, and thus on the flight path angle. This is more efficient than the elevator, which influences the lift force primarily through the angle of attack, causing a time delay in the response.



(a) Time histories of flight path angle γ with DLC off and on. IAS equal to 180 kts, flap setting 1.



(b) Time histories of elevator and DLC flaps deflections.

Fig. 29. Flight test results of flight path angle captures experiments, with and without DLC.

7. Conclusions

This paper has given a comprehensive overview of the basic and advanced principles of various forms of Direct Lift Control (DLC), and clarified the ambiguous terminology around this concept. It has reviewed its commercial, military and experimental implementations, with focus on past and present applications and with reference to simulation and flight test data. It has provided insights into modern scientific literature by making connection between flight control system architectures and control surface layouts made available by different types of aircraft configurations.

DLC — or more generally: Direct Flight Path Control (DFPC) — has to be intended as a means of controlling the lift of an aircraft in the transient dynamic response. It is therefore fundamentally different from the (quasi-)steady combined use of spoilers and auto-throttle employed in civil aircraft operations to control the aircraft attitude, flight path angle, or rate of descent. The type of DLC response fundamentally depends on the position of the Control Center of Pressure (CCoP). Despite being an interesting aerodynamic locus from a theoretical point of view, this point has little practical relevance for the design of a flight control system.

Egregious examples such as the Lockheed 1011 Tristar and the US Navy Precision Landing Mode have clearly demonstrated that flight path tracking accuracy, piloting effort, and passenger comfort can be improved considerably as compared with classical control systems based on Pitch Attitude Control (PAC).

All of the presented applications of DLC use control surfaces already available on the original airframe. Several emerging airframe configurations and advanced control systems, like those using multi-functional moveables, appear to be very well capable of providing DLC capabilities by means of “only” software solutions. Even though the cost of added software functionality may be considerable, this may be easily outweighed by the above merits.

For the near future, a deeper study into handling quality aspects would be useful, as most of the current criteria are more or less

based on moment-controlled aircraft. In order to further look into the potential benefits of emerging airframe configurations, inflight (scaled) demonstration could be a valuable next step.

CRediT authorship contribution statement

Carmine Varriale: Writing – review & editing, Writing – original draft, Visualization, Resources, Project administration, Investigation, Formal analysis, Data curation, Conceptualization. **Thomas Lombaerts:** Writing – review & editing, Writing – original draft, Resources, Investigation, Conceptualization. **Gertjan Looye:** Writing – review & editing, Writing – original draft, Investigation, Conceptualization.

Declaration of competing interest

The authors declare no potential conflicts of interest with respect to the research, authorship, and/or publication of this article.

Data availability

Data will be made available on request.

References

- [1] W.J.G. Pinsker, The Control Characteristics of Aircraft Employing Direct-Lift Control, Reports and Memoranda 3629, Royal Aircraft Establishment Aerodynamics Department, 1968, URL <https://reports.aerade.cranfield.ac.uk/handle/1826.2/2896>.
- [2] L.O. Lykken, N.M. Shah, Direct Lift Control for Improved Automatic Landing and Performance of Transport Aircraft, *J. Aircr.* 9 (5) (1972) 325–332, <http://dx.doi.org/10.2514/3.58988>, Publisher: American Institute of Aeronautics and Astronautics (AIAA).
- [3] J.W. Denham, Project MAGIC CARPET: Advanced controls and displays for precision carrier landings, in: Proceedings of the 54th AIAA Aerospace Sciences Meeting, San Diego, CA, 2016, <http://dx.doi.org/10.2514/6.2016-1770>, no. AIAA-2016-1770.
- [4] D. Reckzeh, Multifunctional wing moveables: Design of the A350XWB and the way to future concepts, in: 29th Congress of the International Council of the Aeronautical Sciences, ICAS 2014, 2014.
- [5] C. Varriale, Flight Mechanics and Performance of Direct Lift Control: Applying Control Allocation Methods to a Staggered Box-Wing Aircraft Configuration (phdthesis), Delft University of Technology, 2022, <http://dx.doi.org/10.4233/uuid:8b868c52-f34f-4307-8fc0-b1176eaf9d04>.
- [6] D. Kohlman, D. Ellis, Direct force control for light airplanes, in: Mechanics and Control of Flight Conference, American Institute of Aeronautics and Astronautics, Anaheim, CA, U.S.A., 1974, <http://dx.doi.org/10.2514/6.1974-862>.
- [7] M. DeSalvo, D. Heathcote, M.J. Smith, A. Glezer, Direct Lift Control using Distributed Aerodynamic Bleed, in: AIAA Scitech 2019 Forum, American Institute of Aeronautics and Astronautics, 2019, <http://dx.doi.org/10.2514/6.2019-0591>.
- [8] D.G. Hull, Fundamentals of Airplane Flight Mechanics, Springer Berlin Heidelberg, 2007, <http://dx.doi.org/10.1007/978-3-540-46573-7>.
- [9] A.A. Lambregts, TECS generalized airplane control system design—an update, in: Advances in Aerospace Guidance, Navigation and Control: Selected Papers of the Second CEAS Specialist Conference on Guidance, Navigation and Control, Springer, 2013, pp. 503–534.
- [10] J.C. Doyle, B.A. Francis, A.R. Tannenbaum, Feedback control theory, 1992.
- [11] B.N. Nield, R.A. Landes, M.R. Evans, Landing attitude modifier for airplane, 1996, URL <https://patents.google.com/patent/US5823479A/en>.
- [12] H. Strüber, The aerodynamic design of the A350 XWB-900 high lift system, in: Proceedings of the 29th Congress of the International Council of the Aeronautical Sciences, 2014, URL https://www.icas.org/ICAS_ARCHIVE/ICAS2014/data/papers/2014_0298_paper.pdf.
- [13] D. Vechtel, B. Hauber, G. Looye, Analysis of a multi-functional high-lift system driven by an active differential gear box, *CEAS Aeronaut. J.* 5 (3) (2014) 227–238, <http://dx.doi.org/10.1007/s13272-014-0102-7>.
- [14] R. König, K.-U. Hahn, J.. Winter, Advanced gust management systems. - lessons learned and perspectives -, in: AGARD-CP-560, 1995, 1995, p. 17, URL <https://elib.dlr.de/30163/>. LIDO-Berichtsjahr=1995.
- [15] T. Lombaerts, G. Looye, Design and flight testing of nonlinear autoflight control laws incorporating direct lift control, in: Advances in Aerospace Guidance, Navigation and Control, Springer Berlin Heidelberg, 2013, pp. 549–568, http://dx.doi.org/10.1007/978-3-642-38253-6_32.
- [16] G. Sim, C. Onspaugh, Laboratory development of selected systems in the lockheed L-1011 TriStar, in: 3rd Aircraft Design and Operations Meeting, American Institute of Aeronautics and Astronautics, 1971, <http://dx.doi.org/10.2514/6.1971-782>.
- [17] G.L. Nelsen, R.C. Lorenzetti, Direct Lift Control for the LAMS B-52 (Master's thesis), School of Engineering of the Air Force Institute of Technology, Wright-Patterson Air Force Base, Ohio, USA, 1968, URL <https://apps.dtic.mil/sti/pdfs/AD0831091.pdf>.
- [18] J.A. Lee, R.P. Johannes, LAMS B-52 flight experiments in direct lift control, in: SAE Technical Paper Series, SAE International, 1969, <http://dx.doi.org/10.4271/690406>.
- [19] R.C. Lorenzetti, G.L. Nelsen, R.W. Johnson, Direct lift control for approach and landing, *J. Aircr.* 6 (3) (1969) 240–244, <http://dx.doi.org/10.2514/3.44042>.
- [20] C.C. Flora, G.K.L. Kriegbaum, W. Willich, A Flight Investigation of Systems Developed for Reducing Pilot Workload and Improving Tracking Accuracy During Noise-Abatement Landing Approaches, *Tech. Rep. NASA-CR-1427*, 1969.
- [21] C. Taylor, Flight Test Results of a Trailing Edge Flap Designed for Direct-Lift Control, NASA Contractor Report NASA-CR-1426, Boeing Co., Seattle, WA, United States, 1969, URL <https://ntrs.nasa.gov/citations/19690029434>.
- [22] L. Rolls, A. Cook, R. Innis, Flight-Determined Aerodynamic Properties of a Jet-Augmented, Auxiliary-Flap, Direct-Lift- Control System Including Correlation with Wind-Tunnel Results, NASA Technical Note NASA-TN-D-5128-REV, NASA Ames Research Center, Moffett Field, CA, United States, 1969, URL <https://ntrs.nasa.gov/citations/19690022584>.
- [23] K. Aoyagi, S. Dickinson, P. Soderman, Investigation of a 0.3-Scale Jet-Transport Model Having a Jet-Augmented Boundary-Layer- Control Flap with Direct-Lift Control Capability, NASA Technical Note NASA-TN-D-5129, NASA Ames Research Center, Moffett Field, CA, United States, 1969, URL <https://ntrs.nasa.gov/search?q=TN-D-5129&reportNumber=NASA-TN-D-5129>.
- [24] M. Gerrits, Direct Lift Control for the Cessna Citation II (Master's thesis), Eindhoven University of Technology, 1995, URL <https://research.tue.nl/en/studentTheses/direct-lift-control-for-the-cessna-citation-ii>.
- [25] A. in't Veld, H. Mulder, G. Looye, Flight tests on fault-tolerant autopilot control laws in laboratory aircraft Citation II, in: Society of Flight Test Engineers – European Chapter Symposium, 2018.
- [26] R. Merat, Study of a direct lift control system based on the A380 aircraft, in: 46th AIAA Aerospace Sciences Meeting and Exhibit, American Institute of Aeronautics and Astronautics, 2008, <http://dx.doi.org/10.2514/6.2008-1432>.
- [27] D. Drake, Direct lift control during landing approaches, in: 2nd Annual Meeting, American Institute of Aeronautics and Astronautics, 1965, <http://dx.doi.org/10.2514/6.1965-316>.
- [28] L. Smith, F. Prilliman, R. Slingerland, Direct lift control as a landing approach aid, in: 3rd and 4th Aerospace Sciences Meeting, American Institute of Aeronautics and Astronautics, New York, NY, U.S.A., 1966, <http://dx.doi.org/10.2514/6.1966-14>.
- [29] J. Stickle, J. Patton, R. Henry, Flight Tests of a Direct Lift Control System During Approach and Landing, NASA Technical Note NASA-TN-D-4854, National Aeronautics and Space Administration, 1968, URL <https://ntrs.nasa.gov/citations/19690001040>.
- [30] Heatblur DCS F-14 Tomcat, Heatblur Simulations, 2019, URL <https://www.heatblur.se/F-14Manual/general.html>. Ch. General Design and Systems Overview.
- [31] R. Fortenbaugh, Practical integration of direct lift control into an automatic carrier landing system, in: Guidance and Control Conference, American Institute of Aeronautics and Astronautics, Stanford, CA, U.S.A., 1972, <http://dx.doi.org/10.2514/6.1972-873>.
- [32] H. Henry, Lockheed S-3 Viking, Plane Encyclopedia, 2022, URL <https://plane-encyclopedia.com/cold-war/lockheed-s-3-viking/>. Ch. Construction.
- [33] D.M. Shafer, R.C. Paul, M.J. King, J.W. Denham, Aircraft carrier landing demonstration using manual control by a ship-based observer, in: AIAA Scitech 2019 Forum, American Institute of Aeronautics and Astronautics, 2019, <http://dx.doi.org/10.2514/6.2019-0010>.
- [34] W.E. McNeill, R.M. Gerdes, R.C. Innis, J.D. Ratcliff, A Flight Study of the Use of Direct-Lift-Control Flaps to Improve Station Keeping During in-Flight Refueling, Technical Memorandum NASA-TM-X-2936, NASA Ames Research Center, 1973, URL <https://ntrs.nasa.gov/citations/19730024237>.
- [35] D. Loebel, M. Weiss, F. Holzapfel, T.Y. Shima, Cooperative docking guidance and control with application to autonomous aerial refueling, in: 2018 AIAA Guidance, Navigation, and Control Conference, American Institute of Aeronautics and Astronautics, 2018, <http://dx.doi.org/10.2514/6.2018-1598>.
- [36] J. Pravitra, E.N. Johnson, Adaptive control for attitude match station-keeping and landing of a fixed-wing UAV onto a maneuvering platform, in: AIAA Scitech 2020 Forum, American Institute of Aeronautics and Astronautics, 2020, <http://dx.doi.org/10.2514/6.2020-1082>.
- [37] W. Mönnich, ATTAS - Flight Test Evaluation. Hermes in-Flight Simulation Test-No. 203, Tech. Rep., 1992, URL <https://elib.dlr.de/29755/>. LIDO-Berichtsjahr=1992.
- [38] D.L. Mallick, P.W. Merlin, The Smell of Kerosene: A Test Pilot's Odyssey, in: NASA History Series, NASA SP Series, no. 4108, National Aeronautics and Space Administration, 2013, URL https://www.nasa.gov/centers/dryden/pdf/88797main_kerosene.pdf.

- [39] W.B. Binnie, R.F. Stengel, Flight investigation and theory of direct side-force control, *J. Guid. Control* 2 (6) (1979) 471–478, <http://dx.doi.org/10.2514/3.55911>.
- [40] S.L. Grunwald, R.F. Stengel, Design and flight testing of digital direct side-force control laws, *J. Guid. Control Dyn.* 8 (2) (1985) 188–193, <http://dx.doi.org/10.2514/3.19958>.
- [41] P.G. Hamel, et al., *In-Flight Simulators and Fly-by-Wire/Light Demonstrators A Historical Account of International Aeronautical Research*, Springer, 2017.
- [42] W.J.G. Pinskyer, Direct lift control, *Aeronaut. J.* 74 (718) (1970) 817–825, <http://dx.doi.org/10.1017/s000192400048430>, Publisher: Cambridge University Press (CUP).
- [43] C. Perkins, R. Hage, *Airplane performance, stability and control*, John Wiley and Sons, 1949.
- [44] F. Beer, E. Johnston, D.F. Mazurek, P. Cornwell, B. Self, *Vector Mechanics for Engineers: Statics and Dynamics* 12th edition, McGraw-Hill, 2019.
- [45] R.C. Hibbeler, *Engineering Mechanics: Dynamics* 14th edition, Pearson Prentice Hall, 2016.
- [46] S. Kim, K.R. Horspool, Nonlinear controller design for non-minimum phase flight system enhanced by adaptive elevator algorithm, in: AIAA Scitech 2020 Forum, American Institute of Aeronautics and Astronautics, 2020, <http://dx.doi.org/10.2514/6.2020-0603>.
- [47] D.L. Kohlman, C.H. Brainerd, Evaluation of spoilers for light aircraft flight path control, *J. Aircr.* 11 (8) (1974) 449–456, <http://dx.doi.org/10.2514/3.60366>.
- [48] A. Tomczyk, Aircraft maneuverability improvement by direct lift control system application, *Aerosp. Sci. Technol.* 9 (8) (2005) 692–700, <http://dx.doi.org/10.1016/j.ast.2005.09.004>, Publisher: Elsevier BV.
- [49] A. Galffy, M. Bock, A. Kugi, Nonlinear 3D path following control of a fixed-wing aircraft based on acceleration control, *Control Eng. Pract.* 86 (2019) 56–69, <http://dx.doi.org/10.1016/j.conengprac.2019.03.006>, Publisher: Elsevier BV.
- [50] W. Durham, K.A. Bordignon, R. Beck, *Aircraft Control Allocation*, Wiley, 2017.
- [51] T.A. Johansen, T.I. Fossen, Control allocation—A survey, *Automatica* 49 (5) (2013) 1087–1103, <http://dx.doi.org/10.1016/j.automatica.2013.01.035>.
- [52] M. Bodson, Evaluation of optimization methods for control allocation, *J. Guid. Control Dyn.* 25 (4) (2002) 703–711, <http://dx.doi.org/10.2514/2.4937>.
- [53] A. Frediani, V. Cipolla, E. Rizzo, The PrandtlPlane configuration: Overview on possible applications to civil aviation, in: Springer Optimization and Its Applications, Springer US, 2012, pp. 179–210, http://dx.doi.org/10.1007/978-1-4614-2435-2_8.
- [54] C. Varriale, M. Voskuijl, A control allocation approach to induce the center of pressure position and shape the aircraft transient response, *Aerosp. Sci. Technol.* 119 (2021) <http://dx.doi.org/10.1016/j.ast.2021.107092>, Publisher: Elsevier BV.
- [55] M. Voskuijl, J.d. Klerk, D.v. Ginneken, Flight mechanics modeling of the PrandtlPlane for conceptual and preliminary design, in: Springer Optimization and Its Applications, Springer US, 2012, pp. 435–462, http://dx.doi.org/10.1007/978-1-4614-2435-2_19.
- [56] ISO 2631-1, Mechanical Vibration and Shock — Evaluation of Human Exposure to Whole-Body Vibration, International Organization for Standardization, 1997, URL <https://www.iso.org/standard/7612.html>.
- [57] C. Varriale, M. Voskuijl, A trim problem formulation for maximum control authority using the attainable moment set geometry, *CEAS Aeronaut. J.* (2021) <http://dx.doi.org/10.1007/s13272-021-00560-4>, Publisher: Springer Science and Business Media LLC.
- [58] W.C. Durham, J.G. Bolling, K.A. Bordignon, Minimum drag control allocation, *J. Guid. Control Dyn.* 20 (1) (1997) 190–193, <http://dx.doi.org/10.2514/2.4018>, Publisher: American Institute of Aeronautics and Astronautics (AIAA).
- [59] R. Stolk, C. de Visser, Minimum drag control allocation for the innovative control effector aircraft, in: 5th CEAS Conference on Guidance, Navigation and Control, 2019.
- [60] R.E. Beck, Application of Control Allocation Methods to Linear Systems with Four or More Objectives (Ph.D. thesis), Virginia Tech, 2002, URL <http://hdl.handle.net/10919/28088>.
- [61] T. Lombaerts, G. Looye, Design and flight testing of nonlinear autoflight control laws, in: AIAA Guidance, Navigation, and Control Conference, American Institute of Aeronautics and Astronautics, 2012, <http://dx.doi.org/10.2514/6.2012-4982>.
- [62] T. Lombaerts, Fault Tolerant Flight Control – A Physical Model Approach (Ph.D. thesis), Delft University of Technology, 2010, URL <http://resolver.tudelft.nl/uuid:538b0174-fe84-43af-954d-02f256b2ec50>.
- [63] T. Lombaerts, J. Kaneshige, S. Schuet, G. Hardy, B.L. Aponso, K.H. Shish, Nonlinear dynamic inversion based attitude control for a hovering quad tiltrotor eVTOL vehicle, in: AIAA Scitech 2019 Forum, American Institute of Aeronautics and Astronautics, 2020, <http://dx.doi.org/10.2514/6.2019-0134>.
- [64] T. Lombaerts, J. Kaneshige, S. Schuet, B.L. Aponso, K.H. Shish, G. Hardy, Dynamic inversion based full envelope flight control for an eVTOL vehicle using a unified framework, in: AIAA Scitech 2020 Forum, American Institute of Aeronautics and Astronautics, 2020, <http://dx.doi.org/10.2514/6.2020-1619>.
- [65] J.-E. Slotine, W. Li, *Applied Nonlinear Control*, Prentice Hall, 1991.
- [66] D. Fischenberg, ATTAS in-Air Aerodynamikmodell, Institutsbericht IB 111-97/31, German Aerospace Center DLR, Institut fuer Flugmechanik, Braunschweig, 1997.